8-2017

Optimization Techniques for the Developing Distribution System

Shane Kimble
Clemson University, shanejkimble@gmail.com

OPTIMIZATION TECHNIQUES FOR THE DEVELOPING DISTRIBUTION
SYSTEM

A Thesis
Presented to
the Graduate School of
Clemson University

In Partial Fulfillment
of the Requirements for the Degree
Master of Science
Electrical Engineering

by
Shane Julian Kimble
August 2017

Accepted by:
Dr. Daniel Noneaker, Committee Chair
Dr. Elham Makram, Co-Chair
Dr. Randy Collins
Dr. Ramtin Hadidi

ABSTRACT

The most rapidly changing part of today's power grid is the distribution system. Many new technologies have emerged that revolutionize the way utilities provide, and now sometimes receive, power to and from their customers. To an extent, the push for de-regulation of utilities has also led to an increased focus on reliability and efficiency. These changes make design and operation of power systems more complex causing utilities to question if they are operating optimally.

Operations Research (OR) is an area of mathematics where quantitative analysis is used to provide a basis for complex decision making. The changing landscape in electric distribution makes it a prime candidate for the application of OR techniques. This research seeks to develop optimization methods that can be applied to any distribution feeder or group of feeders that allows for optimal decisions to be made in a reasonable time frame.

Two specific applications identified in this thesis are optimal reconfiguration during outage situations and optimal location of Battery Energy Storage Systems (BESS). Response to outages has traditionally relied on human-in-the-loop approaches where a dispatcher or a crew working the field decides what switching operations are needed to isolate affected parts of the system and restore power to healthy ones. This approach is time consuming and under-utilizes the benefits provided by widely-adopted, remotely-controlled switching technologies. Chapters Two and Three of this thesis develop a partitioning method for determining the switching operations required to optimize the amount of load that is restored during an event.

Most people would agree that renewable forms of Distributed Generation (DG) provide great benefits to the power industry, especially through reduced impact on the environment. The variable nature of renewables, however, can cause many issues for operation and control of a utilities' system, especially for distribution interconnections. Storage technologies are thought to be the primary solution to these issues with much research focused on sizing and control of BESSs. Equally important for integration, but often overlooked, is the location at which the device is connected. Chapter Four explores this idea by drawing conclusions about optimal BESS location based on well-studied ideas of optimal capacitor location.

DEDICATION

I would like to dedicate this thesis to Dr. Elham Makram and the legacy that she leaves behind at Clemson University after 32 years of tireless efforts to make the power program at Clemson the best in the world. You have been a shining example of what determination, dedication, and commitment to excellence are and I consider myself extremely lucky to have had the chance to study under and learn from you. Enjoy retirement; you've earned it.

ACKNOWLEDGEMENTS

TABLE OF CONTENTS

Table of Contents (Continued)

LIST OF TABLES

LIST OF FIGURES

List of Figures (Continued)

Figure   Page

CHAPTER ONE

INTRODUCTION

1.1 - Motivation for Distribution Optimization

In the preface of his book *Optimization Principles: Practical Applications to the Operation and Markets of the Electric Power Industry*, Narayan Rau discusses the growing need for the use of optimization techniques in power systems that he has noticed over his 40 year career, citing deregulation and new technologies as the major driving forces [1]. Due to the cost prohibitive nature of providing electric utility services, many utilities tend to operate as monopolies. While the absence of competition provides companies with more stable sources of income and allows them to operate more efficiently, the incentive to do so is often removed. Consequently, a large portion of electric utilities have earned reputations with their customers of being inefficient and having poor reliability. As deregulation has begun to make companies understand the importance of providing a good customer experience, coupled with volatile economic times, efficiency and reliability have become focal points of many of today's utilities.

This renewed focus is accompanied by a greater adoption of many technologies that impact today's power grid, particularly at the distribution level where customers are directly connected to the utility. Supervisory Control and Data Acquisition (SCADA) is a system of hardware and software that allows for utilities to operate and monitor their equipment remotely [2]. For distribution systems, this has meant decreased response times for system events and the advent of concepts like Distribution Automation (DA) and self-healing networks.

Distributed Generation (DG) has also had a large impact on areas including metering, distribution reliability, protection, and control [3]. In the case of customer owned DG, the assumption that power will always flow from the utility to the customer is no longer valid. For outage events, DG has functioned as a redundant power source to maintain service to critical customers. In addition, the variability of generation present in renewables forms of DG creates issues with traditional voltage control schemes and has brought about the need for energy storage.

To achieve high reliability and efficiency while simultaneously considering all the effects that new technologies have on design, operation, and maintenance, complicated decisions must be made by utility engineers on a regular basis. Operations Research (OR) is a field of mathematics that has long been used to assist in decision making. In OR, mathematical models are formulated to quantify the outcomes of decisions. Techniques for optimization are then used to find the decision that produces the optimal results. This thesis will focus on Distribution Optimization, the application of OR techniques to distribution systems, and thus a review of the underlying principles of optimization follows.

1.2 - Optimization Principles

There are many classifications of optimization each requiring a different approach to solve. The general form of an optimization problem is shown in (1.1) where $f: \mathbb{R}^n \to \mathbb{R}$ is called the objective function and $X \subseteq \mathbb{R}^n$ is the feasible set.

$$\min_{x \in X} f(x) \tag{1.1}$$

When $X = \mathbb{R}^n$, the problem is called an unconstrained optimization problem. For a smooth function, the minimizer x^* of an unconstrained optimization function will always satisfy the condition $\nabla f(x^*) = 0$. While this condition is necessary, it is not sufficient for optimality without further information related to the convexity of the function. Thus, this condition is known as the first order necessary condition (FONC).

Convexity and KKT Conditions

A function $f: \mathbb{R}^n \to \mathbb{R}$ is convex if and only if it satisfies inequality (1.2). This inequality simply means that for any two points x and y, the function value at any point along the line between x and y, often called a convex combination of x and y, is less than or equal to the linear approximation of the function value at that point.

$$\forall x, y \in \mathbb{R}^n, \forall \lambda \in [0,1], \quad f(\lambda x + (1 - \lambda)y) \leq \lambda f(x) + (1 - \lambda)f(y) \qquad (1.2)$$

An illustration of convexity for $x, y \in \mathbb{R}$ is shown in Figure 1.1. Notice that the line drawn between the points x and y is always above $f(\cdot)$ for the convex case but not for the non-convex case.
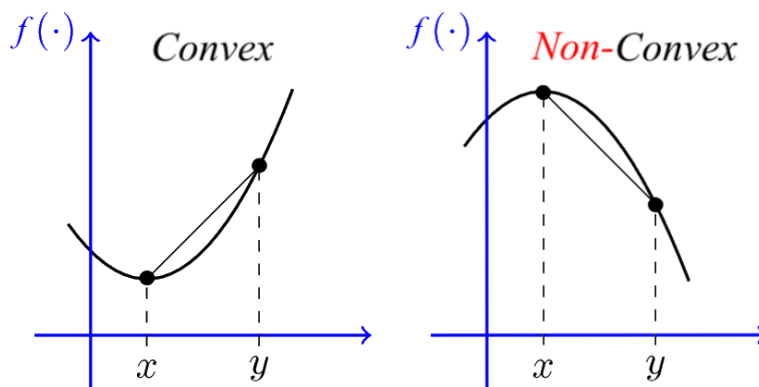
Figure 1.1 – Example of a Convex and Non-Convex Function

Similarly, for a set to be convex, the convex combination of any two points in the set must also be in the set. Figure 1.2 shows an example of a convex and a non-convex set.
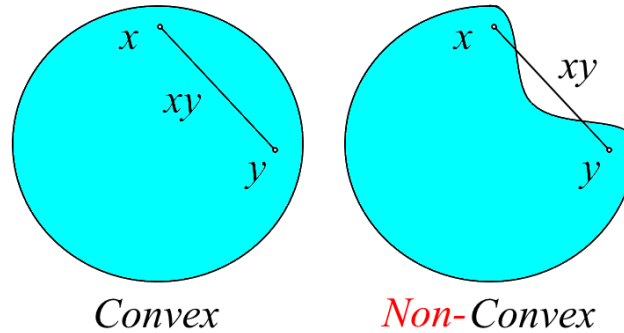
Figure 1.2 – Example of a Convex and Non-Convex Set

In addition to the FONC, for a x^* to be an optimal solution, the function must also be convex at that point. This again is only a necessary condition though and not sufficient, thus the convexity of the function is known as the second order necessary condition (SONC) for optimality. Two conditions do exist that, called the second order sufficient conditions (SOSC), which are sufficient to prove globally optimality. Again, assuming the FONC holds for some x^*, it is sufficient to say x^* is optimal if (a) the function is convex for the entire feasible set X, where X is a convex set, or (b) the function is strictly convex at x^*, a stronger form of convexity defined for a function $f: \mathbb{R}^n \to \mathbb{R}$ by inequality (1.3).

$$\forall x \neq y \in \mathbb{R}^n, \forall \lambda \in (0,1), \quad f(\lambda x + (1 - \lambda)y) < \lambda f(x) + (1 - \lambda)f(y) \qquad (1.3)$$

Since conditions for optimality rely on first and second order information, algorithms for solving these problems will often use this information as well. A typical first order method for finding a minimizer will start at some x_0 in the feasible set and calculate the gradient of the function at that point. The gradient is then used to determine a direction

to travel in and the algorithm will take a step in that direction to a new value x_1. This is repeated until a point is found with a gradient $\nabla f(x^k) \approx 0$ or until an iteration limit is reached. Since this point will only satisfy the FONC, some information about convexity must be known to determine the optimality of the final point.

For constrained optimization where $X \subset \mathbb{R}^n$, it may be true that a global minimizer lies on one of the boundaries of the set X and $\nabla f(x^*) \neq 0$. In this case, the Lagrangian form of the problem is used to determine FONC for optimality. If the set X is defined in the following way, $X = \{x | g_i(x) \leq 0, i = 1, \dots, m\}$, the original problem can be equivalently expressed by (1.4) where λ is known as a Lagrangian dual variable.

$$\min_{x \in \mathbb{R}^n, \lambda \in \mathbb{R}^m} \mathcal{L}(x, \lambda) = f(x) + \sum_{i=1}^{m} \lambda_i g_i(x), \ \lambda_i \geq 0, i = 1, \dots, m \qquad (1.4)$$

Examining the gradient $\nabla \mathcal{L}$ with respect to x, equation (1.5) arises from the FONC as a necessary condition for optimality. For a global minimizer x^*, either $g_i(x^*) = 0$, meaning constraint i is active, or $g_i(x^*) < 0$, meaning constraint i is inactive. For all inactive constraints, it must be true that the corresponding $\lambda_i = 0$. This idea is known as complimentary slackness and is shown in equation (1.6). Finally, original inequalities that define the set X and the non-negative constraints on λ are shown in inequality (1.7).

$$\nabla f(x) - \sum_{i=1}^{m} \lambda_i \nabla g_i(x) = 0 \qquad (1.5)$$

$$\lambda_i g_i(x) = 0, i = 1, \dots, m \qquad (1.6)$$

$$\lambda_i \geq 0, \ g_i(x) \leq 0, \ i = 1, \dots, m \qquad (1.7)$$

Together, these statements are known as the Karush-Kuhn-Tucker (KKT) conditions [1].

Linear Optimization and Integer Optimization

Linear optimization, or linear programming (LP), is a special kind of optimization where the objective function and constraint functions are all linear. Since linear functions are convex, and sets formed from linear inequalities, called polyhedral sets, are convex, any point satisfying the KKT conditions for an LP is an optimal solution. The general form of a LP is shown in (1.8) where $f \in \mathbb{R}^n$, $A \in \mathbb{R}^{m \times n}$, and $b \in \mathbb{R}^m$.

$$\min_{x \in \mathbb{R}^n} f'x \,,\, s.t.\, Ax \leq b \tag{1.8}$$

For any LP over a bounded feasible set, the optimal solution(s) will always occur at an intersection of the hyperplanes forming the boundary of the set. Thus, an algorithm to solve an LP will generally start somewhere in the feasible set and travel along the edges until an optimal solution is found. The Simplex Method is a well-known, fast, and reliable method for solving LPs and there are many commercial solvers available that use some version of it [4].

Because of the reliability and speed of the Simplex Method, it is a common practice to estimate solutions to non-linear optimization problems by linearizing them and using LP techniques to solve. An example in this thesis is the power flow model, specifically the voltage drop calculation. Power flow is inherently a non-linear problem, however, if certain assumptions are made, it can be approximated by linear functions. In Chapter Three, this linearization is discussed in detail and is used to constrain the voltage profile of circuit to fall within a certain range.

Often in real world applications, some variables may be required to be discrete. Two examples are counting problems where the items being counted cannot be divided and

6

decision problems, since many decisions can be represented by binary variables. The Branch & Bound Method is a recursive method that solves sub-problems over a "relaxed" feasible set, meaning the integer constraint is removed, to narrow down the set and arrive at an optimal, integer feasible solution. Figure 1.3 shows a visualization of the branch and bound method for the LP given in (1.9).

$$\min_{x \in Z^2, x \geq 0} -13x_1 - 11x_2 \,, s.t. \begin{bmatrix} 1 & 0 \\ 0 & 1 \\ 2 & 3 \end{bmatrix} x \leq \begin{bmatrix} 4 \\ 4 \\ 15 \end{bmatrix} \tag{1.9}$$
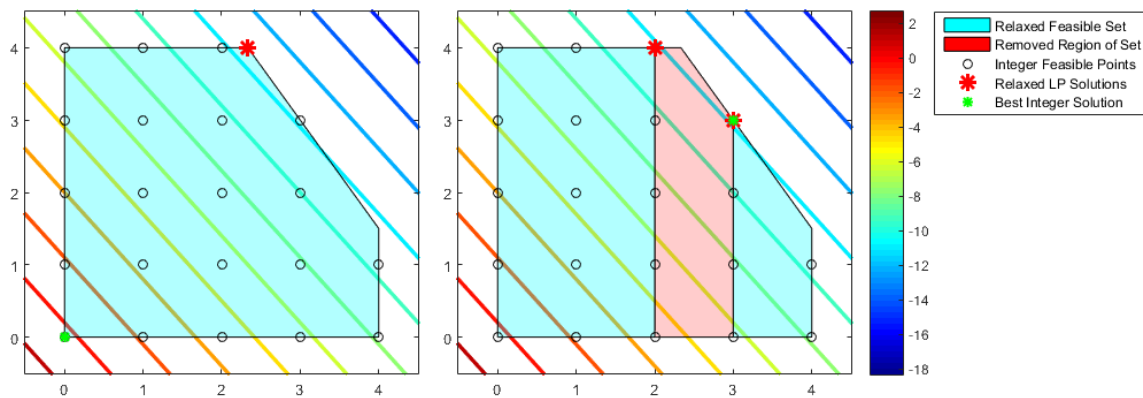
Figure 1.3 – Illustration of the Branch and Bound Method

In the figure, the colored lines represent the level curves of the objective function. Since the objective is to minimize this function, the level curves that are on the blue side of the spectrum are more optimal than the red side. The left side of the figure shows the initial sub-problem that is solved resulting in the red marker. This marker, located at the point $\left(\frac{7}{3}, 4\right)$, is the solution to the LP with the integer constraints removed and thus provides a lower bound on the actual optimal solution. The green marker shows an integer feasible point that is provided to the problem which gives an upper bound for the solution.

The distance between these two bounds is called the relative gap. The Branch and Bound Method converges when the relative gap between an integer feasible solution and the relaxed optimal solution is less than some tolerance [4].

Since the relaxed optimal solution is not integer feasible after the first sub-problem is solved, the problem is then "branched" at $x_1 = \frac{7}{3}$, meaning that two more sub-problems are formed; one with the constraint $x_1 \leq 2$ and the other with the constraint $x_1 \geq 3$. The right side of the figure shows the solutions obtained from solving these two sub-problems. Since the solution $(3,3)$ is integer feasible, it replaces the initial point $(0,0)$ as the lower bound for the problem. In addition, the function value at $(3,3)$ is less than the function value at $(2,4)$ so this point is the new upper bound as well. This results in a relative gap of 0 and thus the method converges at the point $(3,3)$.

IBM's CPLEX is a widely used commercial solver that uses the Branch and Bound Method to solve Mixed Integer Programs (MIPs). Along with Gurobi, CPLEX is regarded as one of the best commercially available softwares for solving MIPs. While the software is not open source and many companies must pay to use it, it is provided free for academic use. All the optimization problems formulated in this thesis require integer constraints for some variables and thus CPLEX is used extensively in this thesis.

1.3 - Thesis Outline

Following this chapter are various applications of the principles described in the previous section to power systems, specifically distribution systems. Chapter Two uses Binary Integer Linear Programming (BILP) to devise a partitioning scheme for distribution

systems during outage situations. The most innovative part of the chapter is the way it uses concepts from graph theory to enforce topological constraints on a graph. The applications of such a partition scheme mainly exist in DA and self-healing networks. Here, the logic can be used to determine switching operations that should occur in response to an event that can re-energize healthy portions of a feeder while leaving the affected areas de-energized. Chapter Three expands on these ideas by considering the ampacity limits of conductors and the variation limits on supply voltage for customers. First, a method is considered for linearizing the power flow calculations and the constraints are enforced internally to the LP. Second, an iterative method is used, where a full power flow is calculated and violations are checked for after the BILP is solved. The arguments for and against each method are discussed and comparisons on application to the partitioning method are made.

Chapter Four discusses the many advantages of inverter based Battery Energy Storage Systems (BESS) which are widely thought to provide a solution to the many issues caused by variability of DG, specifically Photovoltaic (PV) generation. While batteries are a particularly hot topic in academia today, it has become evident to the author that the location of a BESS on a distribution grid is rarely considered. Given that smart inverters can not only send and receive real power to and from the grid, but reactive power as well, there are potentially great benefits to locating batteries in places that allow the BESS to affect the power flowing on a circuit. Considering this, locating a BESS is similar in many ways to locating a capacitor. Thus, Chapter 4 develops a Mixed Integer Quadratic Programming (MIQP) approach for optimally locating a capacitor

which is then developed for a BESS. The BESS location MIQP is applied to a test system

with varying levels of PV penetration and the ability of the BESS to reduce losses on the

system is measured. While using batteries solely as a loss reduction asset does not

generally make a good business case, valuable information regarding locating a BESS is

uncovered through this exercise.

CHAPTER TWO

OPTIMAL PARTITIONING OF DISTRIBUTION NETWORKS FOR MICRO-GRID

OPERATION

2.1 - Introduction

A great concern for the modern distribution grid is how well it can withstand and respond to adverse conditions. One way that utilities are addressing this issue is by adding redundancy to their systems. Likewise, distributed generation (DG) is becoming an increasingly popular asset at the distribution level and the idea of micro-grids operating as standalone systems apart from the bulk electric grid is quickly becoming a reality. This allows for greater flexibility as circuits can now take on exponentially more configurations than the radial, one-way distribution grid of the past. In addition, tools like Supervisory Control and Data Acquisition (SCADA) and Distribution Automation (DA) allow for systems to be reconfigured faster than humans can make decisions on how to reconfigure them. Thus, this chapter seeks to develop an automated partitioning scheme for distribution systems that can respond to varying system conditions while ensuring a variety of operational constraints on the final configuration.

2.2 - Literature Review

Automatic reconfiguration of power systems has been well studied and published in the literature. Fault Location, Isolation, and Service Restoration (FLISR) is an existing group of technologies that seeks to 1) locate faults on the grid, 2) isolate those faults through various means, and 3) reconfigure the system in such a way that can restore power

to the healthy portions of the grid while leaving the damaged portions de-energized. In fact, many utilities currently have FLISR programs integrated into their Distribution Management Systems (DMS) that are used as a reference for system operators. In some cases, utilities have implemented true DA schemes where the FLISR logic is trusted to perform switching operations without a human-in-the-loop [5]. These cases are still relatively rare, however, and usually purposed for research and development of the technology despite consistent evidence that DA can have a significant impact on reducing customer outage frequency and duration [6]. In addition, islanding from the grid and forming a DG-powered micro-grid is still a new idea and the potential benefits of doing so are often not considered by existing FLISR methods.

According to [7], approaches for finding the optimal configuration of a distribution system fall into the following four categories: heuristic methods [8, 9], rule-based approaches [10], genetic algorithms [11], and mathematical programming. The method chosen for this thesis is mathematical programming, thus a review of mathematical programming approaches follows.

Like this thesis, [12] formulates a Linear Program (LP) to solve the reconfiguration problem for distribution systems considering the locations of DG as potential service points. The method in [12], however, can only accommodate radial systems as each edge is directed with a strictly defined parent node. In some configurations, it may be true that power reverses direction causing the opposite node to become the parent node. This is not to say that closed looped configurations should be considered as feasible solutions, but that some optimal configurations may shift the open point of a loop to a new location.

Conversely, [13] uses an approach that treats the network as an undirected graph, thus considering the looped nature of a power system and making all configurations feasible. In this paper, however, the author seeks to partition transmission systems which operate differently from distribution systems. Namely, any configuration considered as a solution in a distribution system needs to be radial which is not the case with transmission systems. Regardless, [13] is a particularly good reference for its use of graph theory to enforce topological constraints on a graph inside of an LP. Similar ideas will be used in this thesis to formulate the problem for distribution systems.

Finally, power flow considerations of the new configuration should be made to ensure that the new state of the system does not overload any of the circuit elements, cause misoperations of protection equipment, or violate any voltage constraints. In [12], a linearized, single-phase formulation for power flow and voltage drop calculations is presented. This formulation is used within an LP to constrain the voltage at each vertex and current flowing through each edge. Conversely, [14] uses a searching algorithm where an unbalanced three-phase power flow is calculated at each iteration of the search. A two-step approach like this can provide a better estimate of the power flow profile in the reconfigured state, however, the reconfiguration problem may have to be solved several times before a solution is found that does not violate any of the power flow constraints. For the initial formulation of the partitioning problem in this chapter, the power flow constraints will be removed from consideration, however, both methods will be explored in further detail in Chapter Three.

In summary, the characteristics of the reconfiguration method presented in this thesis that distinguish it from any methods currently known to the author are the following:

- DG will be considered a potential source for micro-grids to be formed that are islanded from the bulk electric grid.

- The developed method can reconfigure systems containing any number of loops and sources and result in a radial configuration.

- A single micro-grid can connect multiple sources if needed to supply the capacity of the loads.

2.3 - Background Information

To discuss the reconfiguration of a distribution system, it is important to first develop a few ideas in graph theory. The following are definitions for common terms used in graph theory. An **undirected graph** $G(V, E)$ is a collection of vertices V and edges E where the edges are unordered pairs of adjacent vertices. A **path** in G is a sequence of vertices formed by traversing adjacent edges where no edge is passed through twice. A **cycle** is a path that begins and ends on the same vertex. Furthermore, a **cycle basis** C_b is a set of linearly independent cycles from which all the cycles in G can be generated through the disjoint union of any combination of the cycles. A cycle basis is not necessarily unique for any graph, however, the length of any cycle basis for a specific graph will be the same. **Partitioning** a graph is the process of finding a set of disjoint subgraphs $\{G_0, G_1, \ldots, G_K\}$ such that the union $\bigcup_{k=1}^{K} G_k$ equals the original graph G and the intersection $\bigcap_{k=1}^{K} G_k$ is the empty set $\emptyset$. For a subgraph G_k to be **connected**, there must exist a path between every pair

of vertices in the graph. Any graph that is both connected and does not contain any cycles is said to be a **tree**. If the graph does not contain any cycles but is not necessarily connected, the graph is said to be a **forest** or a collection of trees.

In this chapter, two partitions are considered. First the vertices and edges will be separated into active and inactive subgraphs where the active subgraph represents energized portions of the distribution feeder and the inactive, the de-energized portions. In this partition, at least one edge in each cycle is required to be inactive which will ensure that the active subgraph will contain no cycles. Furthermore, the active vertices and edges are partitioned into a set of connected subgraphs making the active subgraph a forest.

The fundamental idea from graph theory that is exploited in this chapter is the relationship between the number of vertices $|V|$, number of edges $|E|$, length of cycle basis $|C_b|$, and number of connected components K that holds true for any undirected graph.

$$|V| - |E| + |C_b| = K \tag{2.1}$$

Equation (2.1) shows this relationship. Here, if the condition $|C_b| = 0$ is forced, the connectivity of the subgraphs of the active elements of G can be ensured given that the number of subgraphs is known.

Forcing $|C_b| = 0$ requires that all the cycles in the original graph are identified. This is accomplished by the following steps: 1) Find a cycle basis of the graph using the Depth First Search (DFS) algorithm. 2) Find all unique disjoint unions of the cycles in the cycle basis. A flowchart for the DFS algorithm is shown in Figure 2.1.
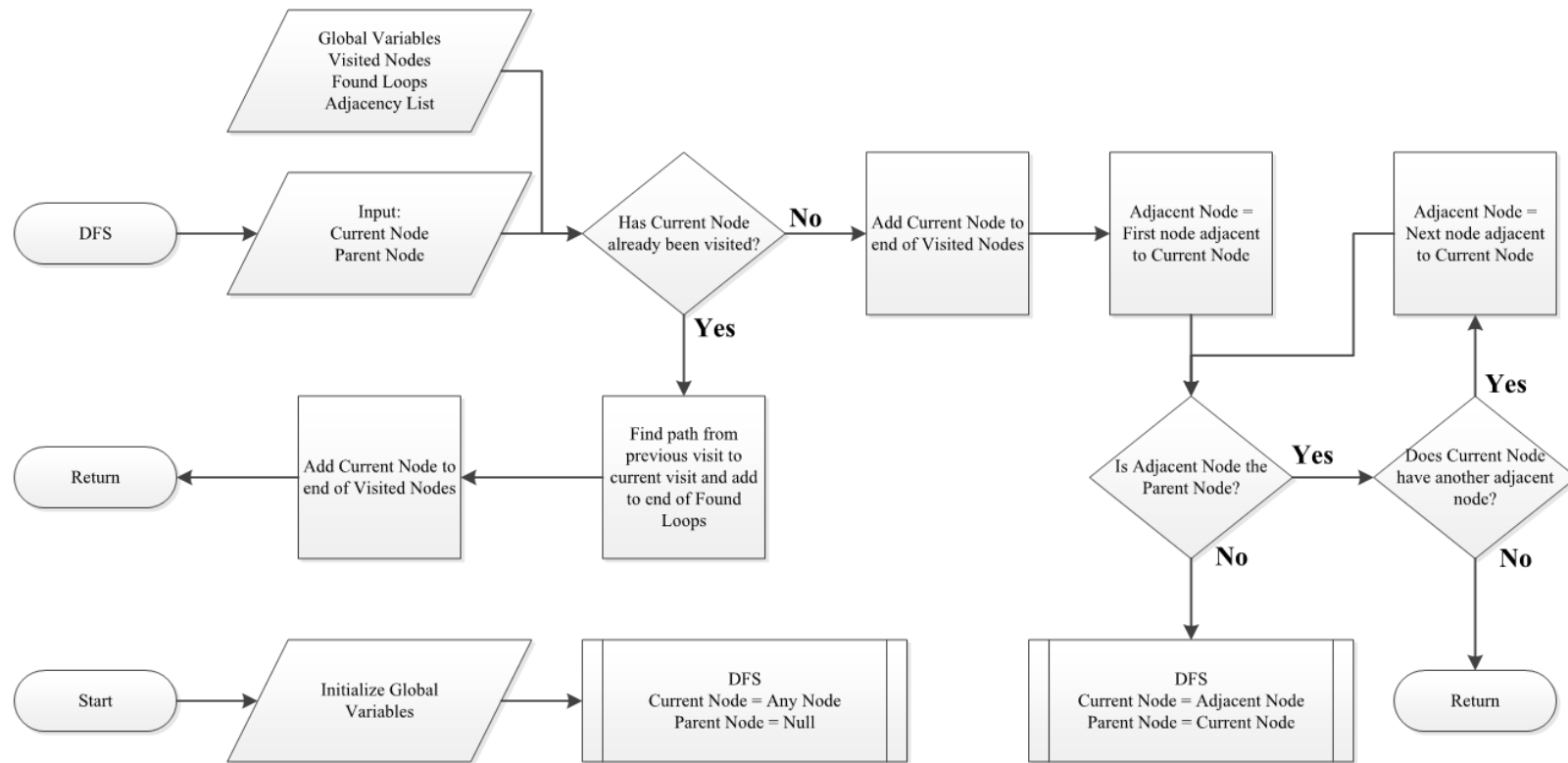
Figure 2.1 − Flowchart for the Depth-first Search Algorithm

The algorithm can start at any node in the graph and traverses the entire graph by scanning adjacent nodes. If any node is visited twice originating from two different paths, a loop is identified. The set of loops that are identified in this manner make up a cycle basis for the graph.

Figure 2.2 shows a simple example of a connected graph containing cycles. In this example, there are (10) vertices and (11) edges, and, since the graph is connected, $K = 1$. Using equation (2.1), $|C_b| = 2$ meaning that a cycle basis will contain exactly two cycles.
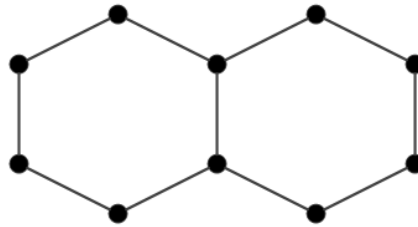
Figure 2.2 – Simple Example of a Graph containing Cycles

In total, however, this graph has three cycles: each of the two hexagons and the edges that form the border of the entire graph. Depending on which node was used as the starting node and how the adjacency list for the graph is formed, DFS would identify any two of these cycles but not the third. Notice, however, that any of the cycles can be formed from the disjoint union of other two cycles. Also, notice that if at least one edge is removed from each cycle, the number of connected components is directly controlled by the number of vertices and edges. This basic example illustrates how topological constraints will be enforced on the graphs used in this chapter.

2.4 - Problem Formulation

Let a distribution system be described by a graph $G = (V, E)$ where each vertex $v \in V$ corresponds to a power distribution pole or pad mount location and the edges $e \in E$ represent the overhead conductors or underground cables that are between any two vertices.

$$V := \{1, \dots, N\} \qquad E := \{(i, j)\} \subset V \times V$$

Here N is the number of vertices in the system and $|E| \leq N^2$. When $|E| \sim N^2$, G is called a dense graph. Power systems, however, usually have much less than N^2 edges and most of the time will satisfy the condition $|E| \leq 2N$, characteristic of a sparse graph.

Sets and Parameters

To further develop the graph G, subsets and parameters for each of the elements are needed. Let the sets L and D be subsets of V containing vertices with loads and sources.

$$L := \{l \in V : a\ load\ is\ served\ from\ vertex\ l\} \subseteq V$$

$$D := \{d \in V : a\ source\ is\ connected\ at\ vertex\ d\} \subseteq V$$

Any given vertex can have a load, a source, both or neither, so the sets L and D are not necessarily disjoint and the union $L \cup D$ does not necessarily contain all of V.

Additionally, let the set C contain all the simple cycles in G found using the DFS.

$$C := \{c_m, m = 1, \dots, M : c_m \subseteq G\ is\ a\ cycle\ in\ G\}$$

Here M is the total number of cycles in G and each $c \in C$ is a subgraph of G. Note that if $|C_b|$ is the number of cycles in a cycle basis of G, then $|C_b| \leq M \leq 2^{|C_b|}$. The set C is not necessarily a partition of G since it may be true that certain vertices or edges belong to multiple cycles while others may not belong to any cycle.

The two partitions discussed at the end of Section 2.3 are defined below.

$$P_1 = \{G^0, G^*\} \qquad P_2 = \{G^k, k = 1, \dots, K\}$$

P_1 is a partition of the graph G into the inactive and active subgraphs, G^0 and G^*, representing the de-energized and energized elements of the circuit respectively. Since a vertex or edge can only be active or inactive, it must be true that $G^* = G \backslash G^0$. P_2 is a partition of the active subgraph G^* where each subgraph G^k is connected and radial, thus forming a tree. Each G^k represents a separate micro-grid that is formed from the original distribution system and thus the subgraphs of P_2 are disjoint. In addition, an edge or vertex must belong to one of these subgraphs for it to be energized so the condition $\bigcup_{k=1}^{K} G^k = G^*$ holds. It is critical to note that the number of subgraphs in P_2 must be less than or equal to the number of sources ($K \leq |D|$) since each micro-grid requires at least one source.

The following notation is used to define the parameters given in the problem.

n_{ij} Normal state for edge (i, j). Each distribution system has a configuration that it takes during normal operation when the entire system is healthy. In this state, the inactive subgraph, G^0, contains the normally open edge for each loop in the system as well as any edges that connect sources which are not normally connected to the circuit. All other edges belong to the active subgraph G^*. n_{ij} is the parameter that identifies the partition P_1 during normal operation in the following way:

$$n_{ij} = \begin{cases} 1 & (i,j) \in G^* \text{ during normal operation} \\ 0 & o.w. \end{cases}$$

p_i, w_i Real power demand and weight for each load $i \in L$ respectively. All loads

will be modeled as constant power loads with demand p_i. The weights are

used to give priority to certain loads. It should be noted that the objective of

the optimization problem is to maximize the total weighted demand that is

active so the weights should be defined in such a way that high priority loads

with a small amount of demand will take precedence over low priority loads

with a large demand.

P_d^R Real power rating for each source $d \in D$.

Variables

Once again, the goal of the problem is to find an optimal partition of the graph G.

Therefore, the variables are defined so that their values depict the partitions P_1 and P_2. This

is accomplished through binary variables that decide whether each vertex or edge belongs

to a given subgraph or not. The maximum number of subgraphs formed by P_1 and P_2 is

equal to the number of sources in G plus one for the inactive subgraph. Thus, each vertex

and edge has $|D| + 1$ binary variables associated with it defined in the following way:

$$a_i^k = \begin{cases} 1 & i \in G^k \\ 0 & o.w. \end{cases} \qquad \forall i \in V, k = 0,1, \dots, |D|$$

$$b_{ij}^k = \begin{cases} 1 & (i,j) \in G^k \\ 0 & o.w. \end{cases} \qquad \forall i \in V, k = 0,1, \dots, |D|$$

It may be possible for $a_i^k = 0 \; \forall i \in V$ and $b_{ij}^k = 0 \; \forall(i,j) \in E$ for some k indicating

that subgraph G^k does not contain any elements. In this situation, the number of connected

subgraphs formed by P_2 is strictly less than the number of sources ($K < |D|$). Since the

number of connected subgraphs is required for the topological constraints discussed previously, a variable is needed to indicate whether each of the subgraphs are empty.

$$d^k = \begin{cases} 1 & G^k \text{ is nonempty} \\ 0 & o.w \end{cases} \qquad k = 1, \dots, |D|$$

In addition, it may be true that a vertex is active, but the load or source located at that node is not. Therefore, a separate variable A is defined for loads and sources.

$$A_i^k = \begin{cases} 1 & a_i^k = 1, \ \text{load/source at } i \text{ is connected} \\ 0 & o.w. \end{cases} \qquad \forall i \in L \cup D, k = 1, \dots, |D|$$

Note that loads and sources located at the same node are not assumed to be linked, so that both can be connected or disconnected individually.

Finally, a variable is needed to track whether an edge has changed states or not.

$$B_{ij} = \begin{cases} 1 & \text{edge } (i,j) \text{ has changed states} \\ 0 & o.w \end{cases} \qquad \forall (i,j) \in E$$

The variable B is critical for obtaining the solution to the problem since the switching operations that need to occur to reach the optimal configuration are stored in this variable.

Assumptions

For the distribution system to be well defined for the reconfiguration problem, certain assumptions are made about each of the elements. First, all sources considered in the set D must be able to be dispatched. This can include gas powered generators, energy storage, potential tie points with adjacent circuits, etc. Sources that cannot be dispatched, such as photovoltaic and wind turbine generation, are not considered because islanding in this manner would cause instability and could damage equipment connected to the islanded grid. Instead, these sources are modeled as a load with a "negative demand" so that their effect on the capacity that a micro-grid can serve is still felt.

Additionally, each edge is assumed to be able to toggle between active and inactive, symbolic of a switch opening or closing. Ultimately, this means that a switch is located on each section of line in the circuit. This is an accurate representation of how underground circuits are as distribution switchgear and pad mounted transformers typically have switches for each of the cable feeds entering or leaving the cabinet. Overhead systems, however, do not normally have switches located between every pole. To account for this, a simplified model of the distribution system is generated by collapsing the sections located in between switches to a single vertex.

Similarly, all edges in the graph must be able to carry three phase power so that a solution where a single or double phase line is reconfigured to carry three-phase load does not occur. Model reduction can also be used to prevent this situation by removing all the single and double phase elements. All the load associated with these elements should be added to the most downstream three-phase vertex in the path between the load and the substation. Alternatively, power flow constraints may also be used to prevent these situations. This idea will be discussed further in Chapter Three.

Objective Statement

The optimal partition is the one that maximizes the total load that is re-energized, weighted so that critical loads are considered first, while executing the minimum number of switching operations. Thus, the problem is bi-objective. The following summation quantifies the first objective, the total weighted load belonging to an active subgraph:

$$\sum_{i \in L} w_i p_i \sum_{k=1}^{|D|} A_i^k$$

Here $w_i p_i$ is only counted if $A_i^k = 1$ for some k. The second objective, minimizing the

number of switching operations required to reach the reconfigured state, is used to prevent any unnecessary switching from occurring (i.e. moving an open point to another location on a healthy loop). The number of switching operations are counted using the variable B.

$$\sum_{(i,j)\in S} B_{ij}$$

Maximizing the first objective is equivalent to minimize the additive inverse, thus the two objectives are summed into a single minimization state shown in (2.2). A regularization parameter λ is used to adjust the relative weights of each objective.

$$\min_{a,b,A,B,d} -\left(\sum_{i\in L} w_i p_i \sum_{k=1}^{|D|} A_i^k\right) + \lambda\left(\sum_{(i,j)\in S} B_{ij}\right) \tag{2.2}$$

It is important to note that the switching objective criteria is secondary to the weighted load criteria, and thus the regularization parameter should be tuned in such a way that de-energizing a load is costlier than preventing a switch from toggling.

Constraints

The constraints of the problem fall into three separate categories. The Distribution System Condition Constraints (DSCS) [(2.3) & (2.4)] ensure that the unhealthy portions of the feeder are de-energized (belong to the inactive sub-graph). The Switching Variable Constraints (SVC) [(2.5) – (2.10)] constrain the relationships between the variables a, b, A, and B due to switching. Finally, the Subgraph Connectivity and Radiality Constraints (SCRC) [(2.11) – (2.19)] require all active subgraphs formed by partition P_2 to be connected and radial. An explanation of each follows.

23

1. Distribution System Condition Constraints:

Consider the initial condition of the Distribution System at the time of reconfiguration. Certain vertices or edges may be inoperable due to faulty conditions. Let all such vertices and edges be in the sets V^0 and E^0 respectively. Equations (2.3) and (2.4) will force these elements to be in the inactive subgraph G^0.

$$a_i^0 = 1, \forall i \in V^0 \tag{2.3}$$

$$b_{ij}^0 = 1, \forall (i,j) \in E^0 \tag{2.4}$$

2. Switching Variable Constraints:

The variable A is related to the variable a by the condition that a load cannot be connected to a subgraph unless the vertex that it is located at also belongs to that subgraph. Inequality (2.5) ensures that A is less than or equal to a satisfying this condition.

$$A_i^k \leq a_i^k, \forall i \in L \cup D, k = 1, \dots, |D| \tag{2.5}$$

Similarly, B is the variable that tracks whether an edge has changed states. Equation (2.6) uses an absolute value to describe this relationship where $\sum_{k=1}^{|D|} b_{ij}^k$ indicates if edge (i,j) belongs to an active subgraph and n_{ij} indicates its status under normal operation.

$$B_{ij} = \left| \sum_{k=1}^{|D|} b_{ij}^k - n_{ij} \right|, \forall (i,j) \in E \tag{2.6}$$

Equivalently, this statement is rewritten using the following linear inequality constraints:

$$B_{ij} \leq \sum_{k=1}^{|D|} b_{ij}^k + n_{ij}, \forall (i,j) \in E \tag{2.7}$$

$$B_{ij} \geq \sum_{k=1}^{|D|} b_{ij}^k - n_{ij}, \forall (i,j) \in E \tag{2.8}$$

$$B_{ij} \geq n_{ij} - \sum_{k=1}^{|D|} b_{ij}^k, \forall (i,j) \in E \tag{2.9}$$

$$B_{ij} \leq 2 - \sum_{k=1}^{|D|} b_{ij}^k - n_{ij}, \forall (i,j) \in E \tag{2.10}$$

3. Subgraph Connectivity and Radiality Constraints:

For a subgraph to be active, it must contain a source. Furthermore, the capacity of the sources contained by a subgraph must be sufficient to supply all the loads contained in the same subgraph. Inequalities (2.11) and (2.12) forces d^k to track whether G^k contains a source or not and inequality (2.13) ensures the capacity constraint is satisfied.

$$d^k \leq \sum_{i \in D} A_i^k, k = 1, \dots, |D| \tag{2.11}$$

$$d^k \geq A_i^k, \forall i \in D, k = 1, \dots, |D| \tag{2.12}$$

$$\eta \sum_{i \in L} A_i^k p_i / pf \leq \sum_{i \in D} A_i^k P_i^R, k = 1, \dots, |D| \tag{2.13}$$

Here η is a multiplier to estimate the power losses and pf is a "worst case" power factor for the source.

Equations (2.14) and (2.15) ensure that P_1 and P_2 meet the two requirements of being a partition: 1) all subgraphs are disjoint and 2) the union of all subgraphs is the original graph. This is accomplished by setting the sum of the binary variables a and b over all subgraphs $k = 0, 1, \dots, |D|$ equal to one for every vertex and edge respectively.

$$\sum_{k=0}^{|D|} a_i^k = 1, \forall i \in V \tag{2.14}$$

$$\sum_{k=0}^{|D|} b_{ij}^k = 1, \forall (i, j) \in E \tag{2.15}$$

Furthermore, for an edge to belong to G^k, each of the vertices adjacent to that edge must also belong to G^k unless the edge is inactive. Inequality (2.16) restricts b_{ij}^k to be zero unless both a_i^k and a_j^k are both one. Note that an edge can remain inactive even if both adjacent vertices belong to the same subgraph as is the case with open points in a loop.

$$2b_{ij}^k \leq a_i^k + a_j^k, \forall (i, j) \in E, k = 1, \dots, |D| \tag{2.16}$$

Likewise, if a vertex belongs to a subgraph, there must exist an edge connected to that vertex also in the subgraph. Inequality (2.17) restricts a_i so that this condition is met.

$$a_i^k \leq \sum_{(ij) \in E} b_{ij}^k + \sum_{(j,i) \in E} b_{ji}^k, \forall i \in V, k = 1, \dots, |D| \tag{2.17}$$

Finally, to ensure that the solution of the BILP is radial, the set of active vertices and edges must form a forest. Inequality (2.18) will break each cycle by ensuring at least one edge is inactive and equation (2.19) invokes equation (2.1) by counting the number of vertices, edges, and non-empty subgraphs of G^* using variables a, b, and d respectively.

$$\sum_{(i,j) \in c_m} \sum_{k=1}^{|D|} b_{ij}^k \leq |c_m| - 1, m = 1, \dots, M \tag{2.18}$$

$$\sum_{i \in V} \sum_{k=1}^{|D|} a_i^k - \sum_{(i,j) \in E} \sum_{k=1}^{|D|} b_{ij}^k = \sum_{k=1}^{|D|} d^k \tag{2.19}$$

2.5 - Results and Discussion

Table 2.1 shows specifications for the three test systems pictured in Figure 2.3 on the following page. In the table, $|V|$ is the number of vertices, $|E|$ edges, $|C_b|$ length of a cycle basis, $|L|$ the number of loads, and $|D|$ the number of sources. Test Systems 2 and 3 are actual utility circuit models. The former is a single distribution circuit located in a suburban area, and the latter is an entire substation model located in a rural area. These test systems are used throughout Chapters Two and Three.

Table 2.1 – Test Distribution System Specifications

System Name	Source	$|V|$	$|E|$	$|C_b|$	$|L|$	$|D|$
Test System 1 (a)	IEEE 69-Bus System	75	79	5	48	5
Test System 2 (b)	Local Utility	675	688	14	289	5
Test System 3 (c)	Local Utility	4700	4735	36	2536	10

(a) Test System 1

(c) Test System 3

Source
Load
Normally Open Section
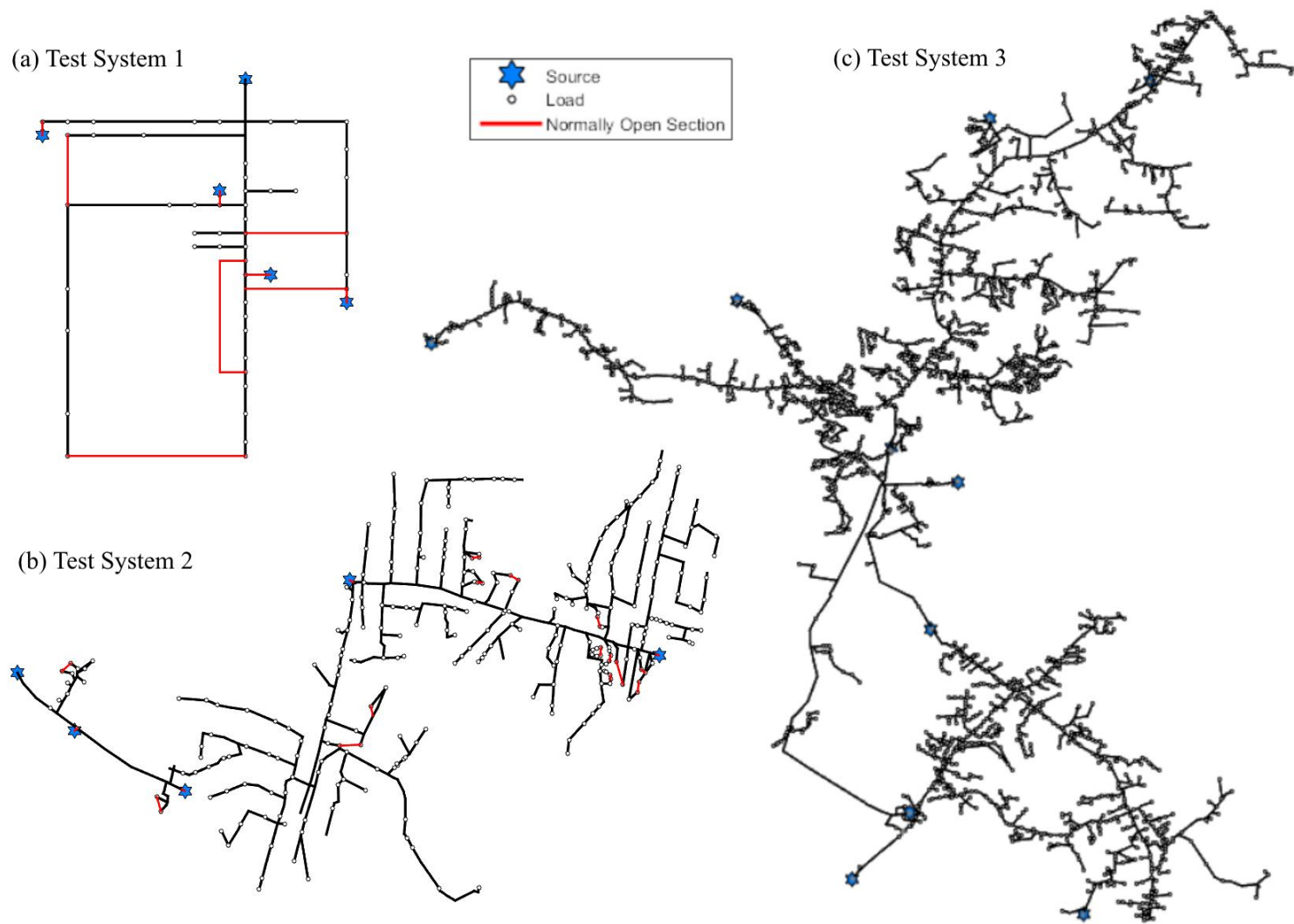
(b) Test System 2

Figure 2.3 – Test Distribution Systems

For Test System 1, all section are assumed to be switchable, however, Test Systems 2 and 3 have (148) and (840) switchable devices respectively, thus model reduction can be used on these systems. The distributed source locations marked by the blue stars in Figure 2.3 were given for Test System 1, however, Test Systems 2 and 3 were modified so that they would have more sources. Most of these locations were identified as probable points of interconnection with adjacent circuits with the exception of three known DG installations on Test System 3. All three of these DG sources are PV farms, however, it was assumed that battery storage was located at each for the purposes of this thesis.

To validate the BILP formulation a variety of fault situations are placed on each test system and the BILP is solved. For each case, CPLEX is called from the MATLAB interface using the OptiToolbox to solve the BILP on a PC with an Intel Core i5-4590 3.3GHz processor and 8GB of RAM. An interpretation of the results follows.

Test System 1

The IEEE 69-Bus Test System is unique for its looped nature. The (5) cycles in the basis of the graph combine to form a total of (26) unique simple cycles. For this test system, the BILP is formulated and solved for four different scenarios. Scenario (a) is the normal operation case in which no faults are present on the system. Scenarios (b) and (c) and the single main-line fault and multiple main-line faults situations where random edges in the graph are selected as faulted and unfit for operation. Finally scenario (d) was designed by selected certain edges to be faulty so that the results would connected multiple sources to a single micro-grid. The results, pictured in Figure 2.4, show the partitions generated from each scenario represented by the different color lines.

(a) Normal Operation

(b) Single Main-Line Fault

(c) Multiple Main-Line Faults

(d) Multiple Sources in One Micro-grid
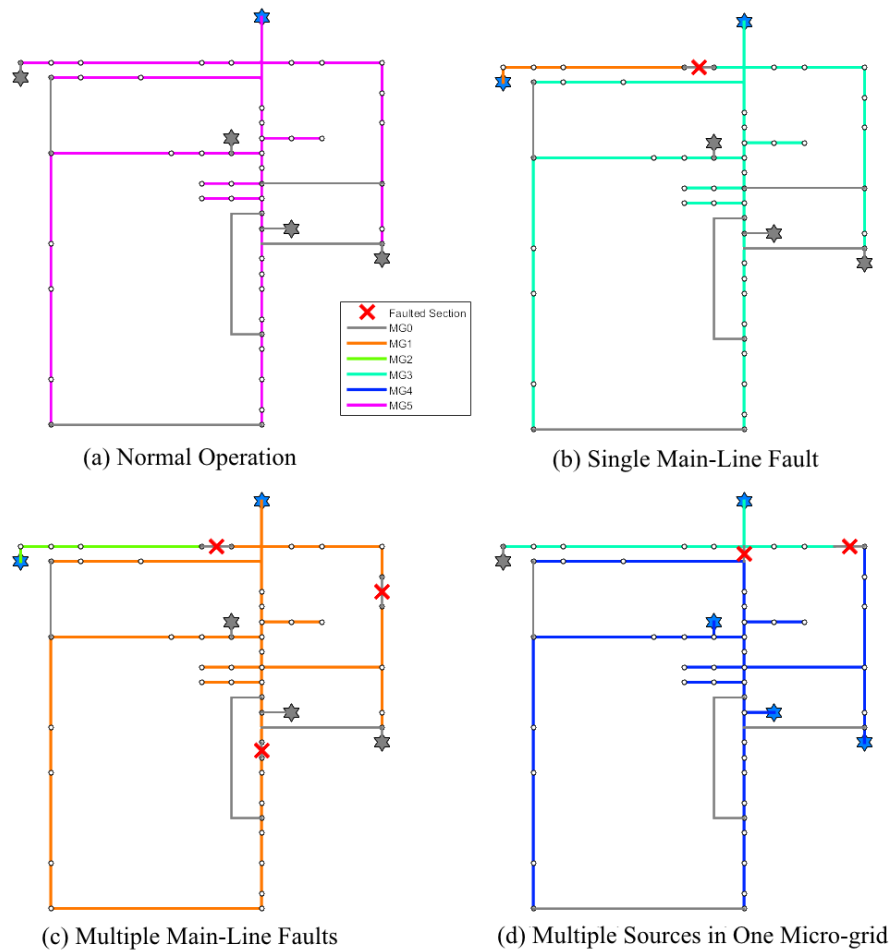
Figure 2.4 – BILP Results for Test System 1

Note that for scenario (a) the normal state for each edge and source is returned. The top source, representing the substation bus, is the only source active in the test case. Comparing this case to (b) – (d) it can be see that most normally open sections remain open. This shows the effectiveness of enforcing the switching criteria in the objective function and verifies that excessive switching is not occurring. Also, notice the ability of the method to add multiple sources to a single micro grid in scenario (d). For this scenario, most of the system was isolated form the normal feed and the capacity of the three

29

distributed sources were adjusted so that each would need to be active to supply the isolated loads. As expected, each source is energized and all the system load is restored.

Convergence results of the BILP for the 69-Bus Test System are shown in Table 2.2. The method performs well for a system of this size and is shown to easily handle the high number of cycles. Additional faults did not have a large impact on convergence, demonstrated by the similarity in solution time between scenarios (b) and (c). Scenario (d) took the most time to converge with a solution time of 2.18 seconds. This was also the only scenario that did not find an integer optimal solution, but instead converged by reaching the relative gap tolerance.

Table 2.2 – Test System 1 Convergence Results

Test Case	Converged	Relative Gap	Solution Time
Normal Operation	Int. Optimal	0	0.2383 s.
Single Main-Line Fault	Int. Optimal	0	0.3331 s.
Multiple Main-Line Faults	Int. Optimal	0	0.3035 s.
Micro-grid w/ Multiple Sources	Gap Tol.	5.5619e-05	2.1847 s.

Test System 2

Next, the reconfiguration problem was tested on Test System 2, the suburban distribution circuit received from a local utility. This circuit is very load dense and has many tie locations with adjacent circuits. In addition, the circuit features many lateral underground loops forming a total of (16) unique simple cycles. Using the same four scenarios to test this system, the BILP was formulated and solved.
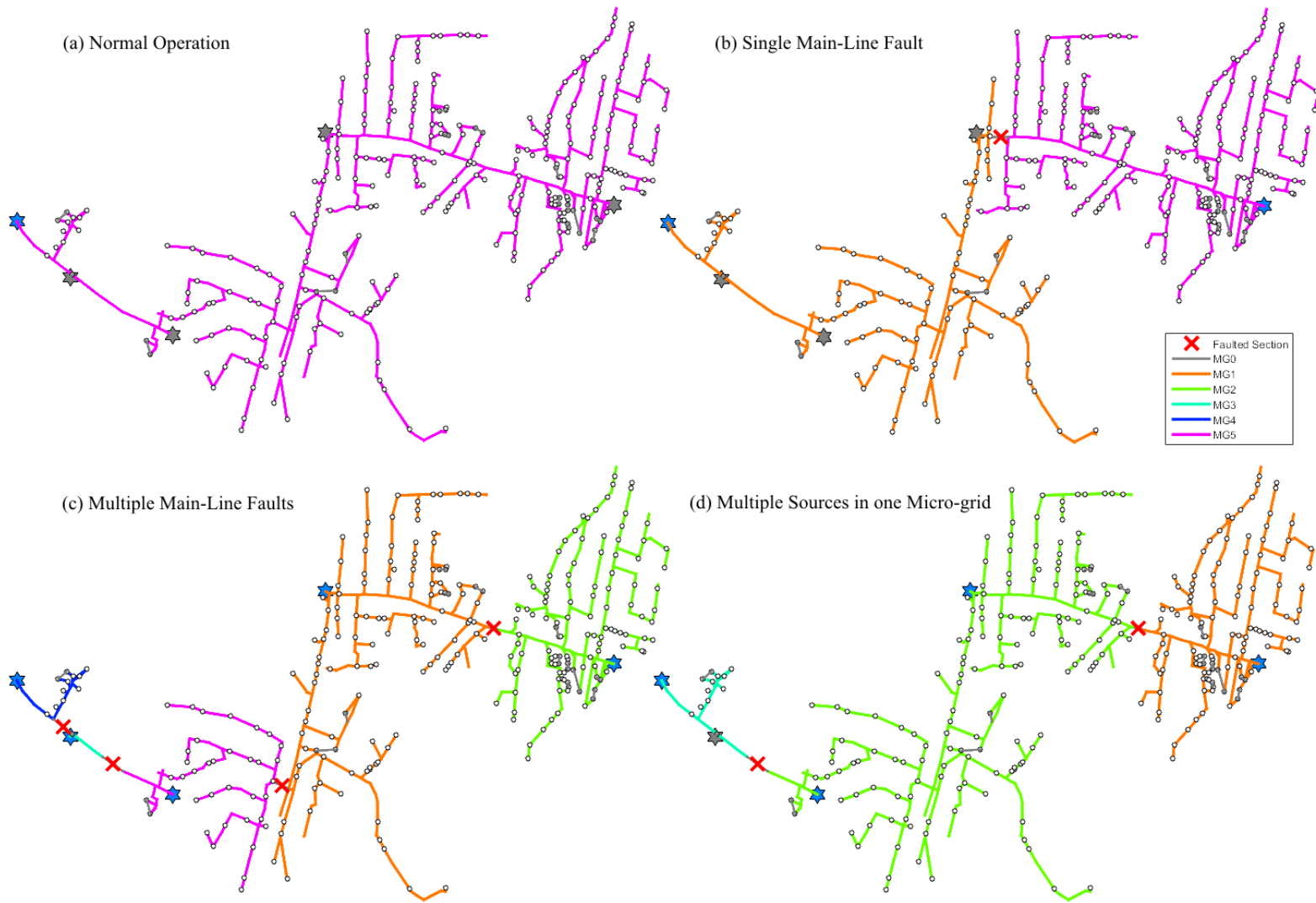
Figure 2.5 – BILP Results for Test System 2

Results are shown in Table 2.3 and Figure 2.5 and are like the results achieved from Test System 1. The system was configured correctly under normal operation, isolation of both the single main-line fault and multiple main-line faults occurred properly, and the algorithm was able to assign multiple sources to a single grid when necessary.

Table 2.3 – Test System 2 Convergence Results

Test Case	Convergence	Relative Gap	Solution Time
Normal Operation	Int. Optimal	0	135.00 s.
Single Main-Line Fault	Int. Optimal	0	170.13 s.
Multiple Main-Line Faults	Int. Optimal	0	205.54 s.
Micro-grid w/ Multiple Sources	Gap Tol.	1.8059e-05	504.75 s.

The largest difference between Test Systems 1 and 2 is the time required to solve the BILP. The dramatic increase in solution time shown in Table 2.3 from the previous test system is a direct result of the increase in the number of vertices and edges in Test System 2. This underscores the importance of model reduction before the LP is solved. As discussed previously in this chapter, it must be assumed that all edges defined in G are switchable. Since this is not the case for this system, adjacent sections can be grouped together when they cannot switch independently. This type of model reduction is shown in Figure 2.6 for Test System 2. After reduction the circuit has only (48) nodes, (49) sections, (2) loops, and (49) switchable devices. In addition, the reduced model more accurately represents the circuit with respect to reconfiguration since only those sections which can be switched remain in the graph.
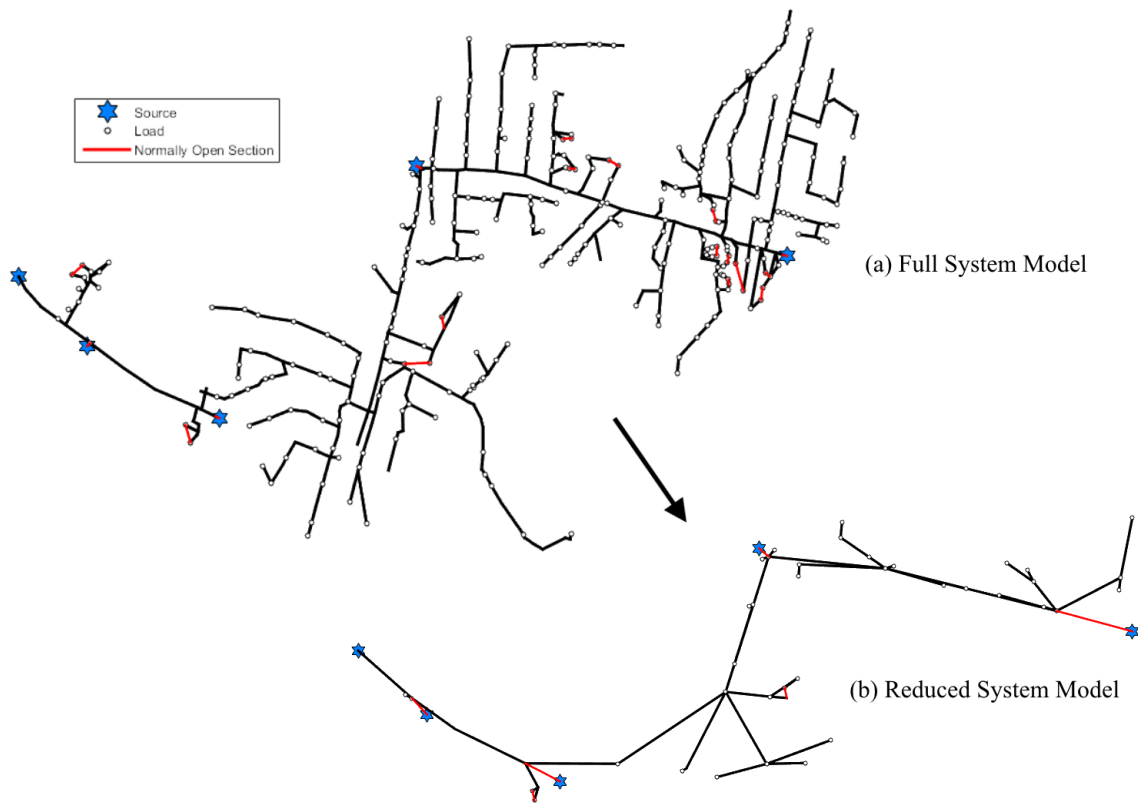
Figure 2.6 – Test System 2 Model Reduction

Using this reduced model, a new solution is calculated for the single main-line fault scenario and then projected back to the original circuit. The results of this is shown in Figure 2.7. Notice that a much larger amount of the circuit is left inactive in this result than in the result from the original graph. This is due to the decreased resolution of the switch locations that results from model reduction. The entire grey section of the circuit in Figure 2.7 corresponds to a single vertex in the reduced graph. The BILP converged to an integer optimal solution in 0.1884 s, a large improvement from the 170 s taken to solve the single main-line fault for the full system model.
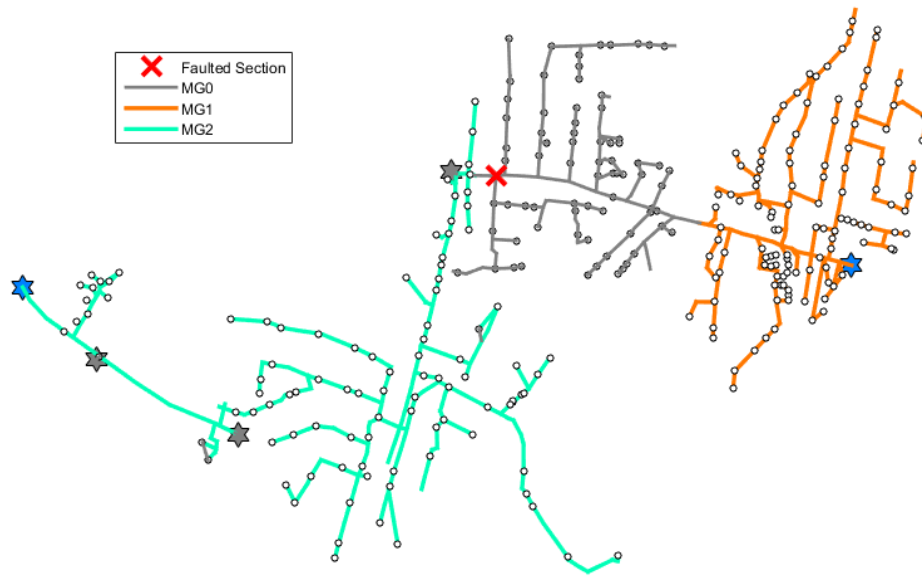
Figure 2.7 – Single Main-Line Fault on Test System 2 Reduced Model

Test System 3

Finally, the BILP was applied to Test System 3, the full substation model. Using a similar reduction technique as before, Test System 3 reduces to (48) nodes, (53) sections, and (6) loops in the cycle basis forming (20) unique cycles. Figure 2.8 shows the original model (a) and reduced model (b). In addition to grouping adjacent edges, all laterals have been collapsed down to the main-line node which they are associated with. This is because laterals are typically radial and protected with fuses or reclosers. If a fault were to occur on a lateral, the protection equipment would automatically isolate the fault and the lines could not be re-energized until the repair is complete. Further reducing the system in this way allows for the problem to only consider reconfiguration of the backbone of the distribution feeders and can decrease the time required for the solver to converge.
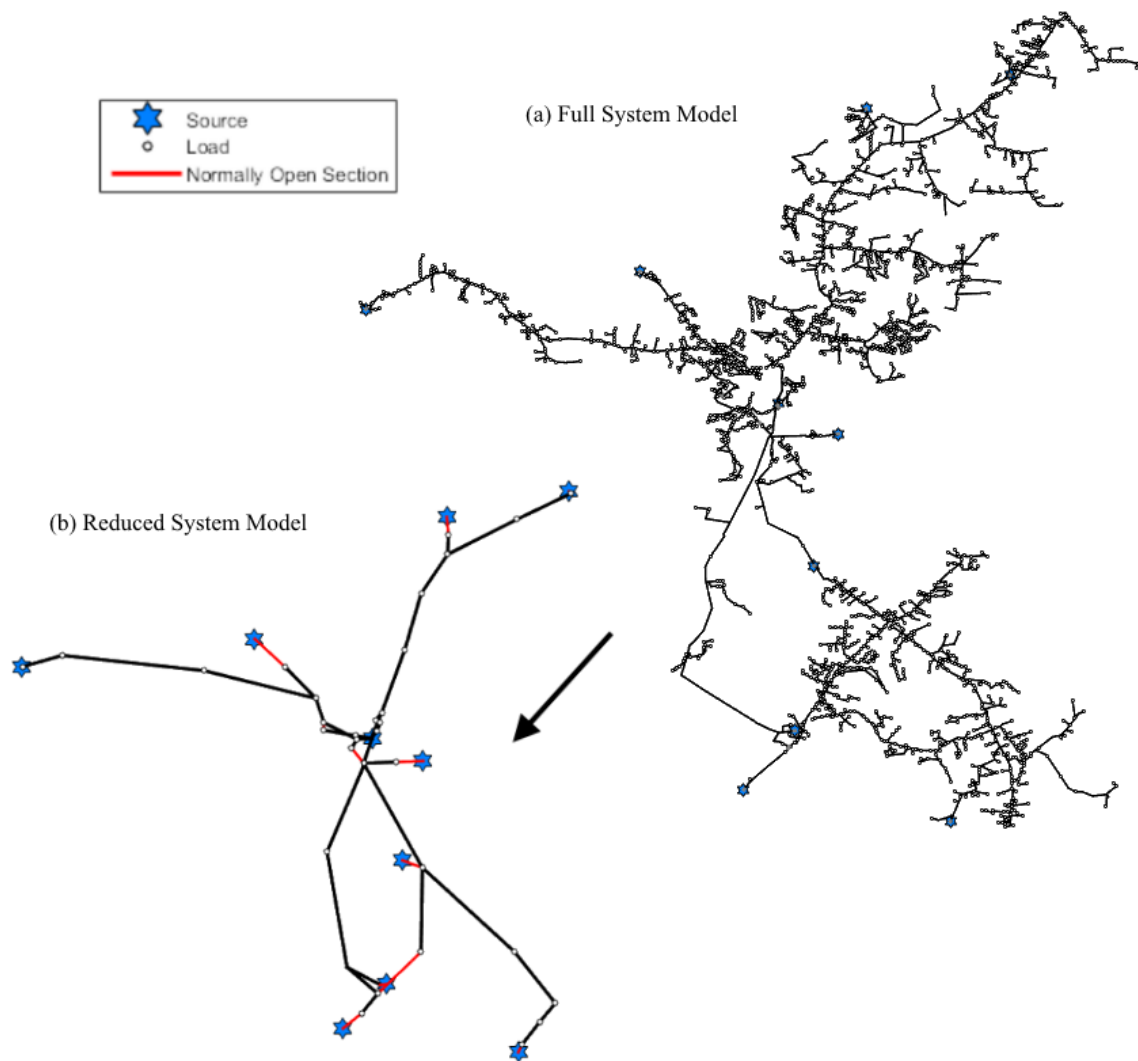
Figure 2.8 – Test System 3 Model Reduction

Figure 2.9 on the following page shows the four cases that were simulated for Test System 3: (a) normal operation, (b) single main-line fault, (c) three main-line faults, and (d) ten main-line faults. In each case, the correct configuration was found. Cases (b), (c), and (d) all require a circuit tie switch to be closed in and cases (c) and (d) require (11) and (15) switching operations respectively.

(a) Normal Operation

(b) Single Main-Line Fault

(c) Three Main-Line Faults

(d) Ten Random Fault Locations

Faulted Section
MG0
MG1
MG2
MG3
MG4
MG5
MG6
MG7
MG8
MG9
MG10
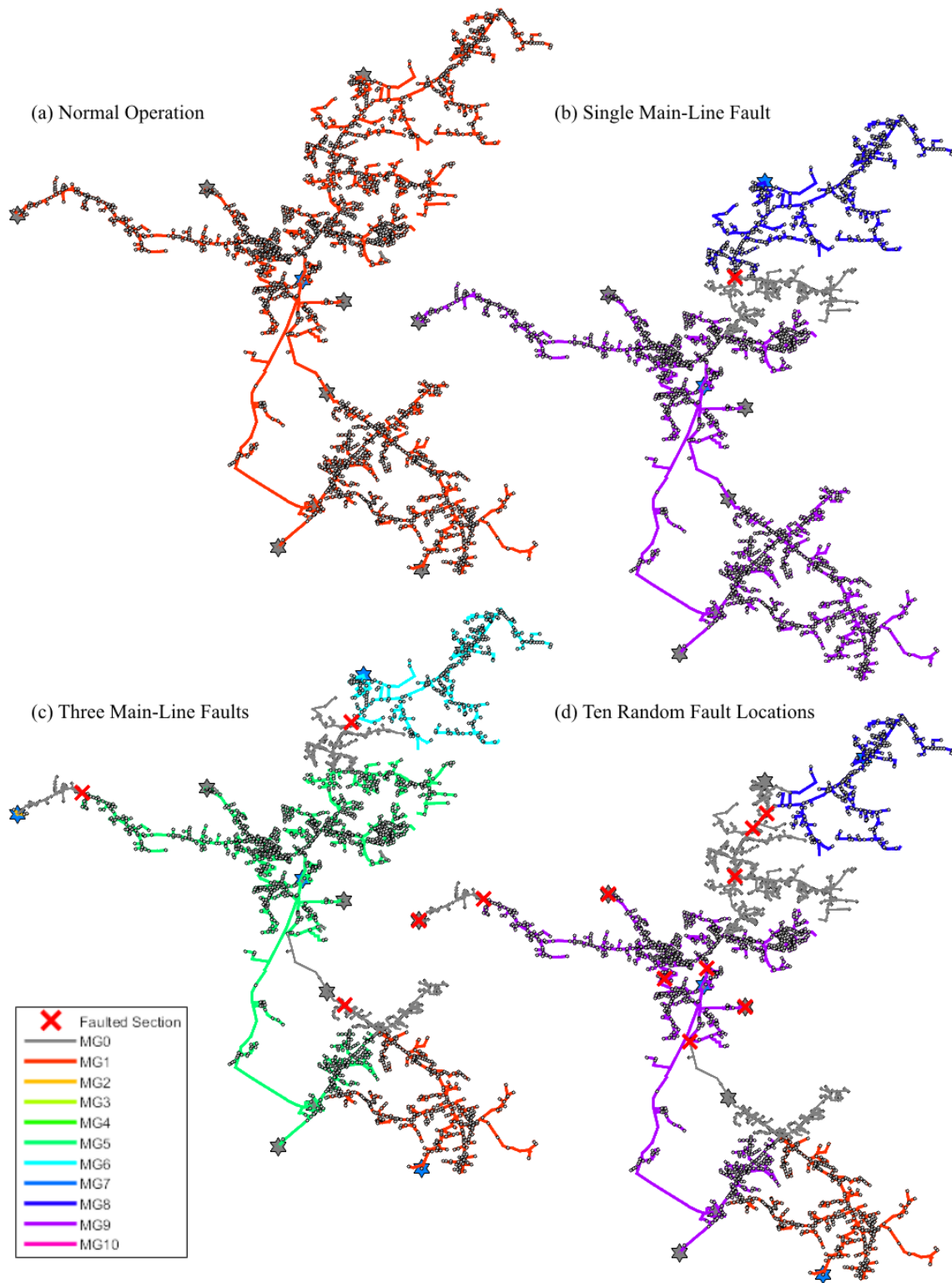
Figure 2.9 – BILP Results for Test System 3 Reduced Model

Likewise, convergence results are shown in Table 2.4. All cases converged from finding an integer optimal solution. Case (b) took the longest to converge at 0.8270 s. All times are well within the constraints to partition a power system in real time. This demonstrates the effectiveness of the method even for large scale substation models and complicated system events.

Table 2.4 – Test System 3 Reduced Model Convergence Results

Test Case	Convergence	Relative Gap	Solution Time
Normal Operation	Int. Optimal	0	0.1831 s.
Single Main-Line Fault	Int. Optimal	0	0.8270 s.
Three Main-Line Faults	Int. Optimal	0	0.1887 s.
Ten Random Fault Locations	Int. Optimal	0	0.1431 s.

2.6 - Conclusion

In this chapter, linear programming and graph theory were used to create a partitioning method for distribution systems during outage events. The problem was formulated as a BILP and applied to three different test systems of varying size and for several different faulted scenarios. In each case, the method performed favorably and the optimal system configuration was found. Most notably, the constraints to enforce radiality on the graph were shown to be effective. Larger test systems adversely affect the time required for the BILP to converge, however, using model reduction, all solution times were reasonable for use in a real-time FLISR scheme. In the following chapter, power flow considerations are made to verify the results of the BILP.

CHAPTER THREE

POWER FLOW CONSIDERATIONS FOR THE OPTIMAL PARTITIONING

SCHEME

3.1 - Introduction

In the previous chapter, a BILP was developed for optimally partitioning distribution systems into micro-grids during outage situations. Motivation for this BILP comes from the growing amount of Distribution Automation (DA) implemented by utilities and the increased complexity that Distributed Generation (DG) adds to the reconfiguration problem. The key features of the partitioning method are that systems with any number of loops or sources are accommodated and that multiple sources can be connected to a single micro-grid to ensure enough generation capacity. For the formulation of the BILP, however, power flow considerations are neglected. This chapter seeks to validate the feasibility of solutions to the partitioning scheme from the previous chapter by ensuring that certain power flow constraints are met.

3.2 - Background Information

In electrical distribution systems, there are several quality metrics and power flow constraints that system operators and designers must consider. Typically, for switching to occur on a distribution system, a request will be made to a distribution dispatch center. The switching operations will then be simulated using some type of power flow analysis software. The two most crucial constraints that are checked before any switching is approved are overloading conditions, and under voltage conditions. Stability and transient

issues should also be considered when partitioning power networks, especially when operating micro-grids islanded from the bulk power grid, however, these issues are not often studied with respect to distribution switching and are beyond the scope of this thesis.

Overloading of a circuit element is a condition where the rated current or rated power on that element is exceeded. This can occur on many different types of equipment, however, it is most common to check for overloading on transformers and conductors. Typically, a distribution circuit will have protection equipment that operate before any upstream devices are damaged, but with increased use of DG, the "upstream" direction of a device is not as definite and thus protection coordination is not always reliable. To check for overloading conditions in a reconfigured circuit, each line's ampacity rating will need to be considered in addition to the operating points of the protective devices.

Ampacity ratings for conductors are a function of the thermal limits of the conductor material. As current flows through a wire, the resistive losses, or I^2R losses, generate heat. If enough current flows in the wire for an extended amount of time, the temperature of the conductor will reach a critical point and the conductor will fail. Each conductor will typically have three different ampacity ratings related to the time-frame in which the respective rated current can pass through the conductor without failure: normal – continuous operation, long term emergency (LTE) – emergencies limited to 3 hours, and short term emergency (STE) – emergencies limited to 15 minutes. Ambient temperature and weather conditions also affect ampacity rating due to the heating or cooling effect on the conductor. Ampacity ratings are given in Table 3.1 for several common conductors at the standard operating conditions: conductor at 65°C, air at 95°F, and wind at 2ft/s.

Table 3.1 – Standard Conductor Ratings

Conductor Size	Normal Ampacity	LTE Ampacity	STE Ampacity
477 ACSR-26/7	495 A	569 A	653 A
4/0 ACSR-6/1	280 A	322 A	396 A
#2 ACSR-6/1	140 A	161 A	185 A
336 AAC-19	480 A	552 A	633 A
4/0 AAAC-7	390 A	448 A	515 A

Protection schemes are designed for specific operating conditions related to current and thus the constraints for preventing unwanted operations are easier to define. Breakers, reclosers, and fuses can all be characterized by their Time-Current Characteristic (TCC) curves which shows the time that the device will take to operate as a function of the amount of current flowing through it.

Figure 3.1 shows a typical distribution system (a) and the coordination of the breaker, recloser, and fuses in that system using their TCC curves (b). Here, the Recloser S and Recloser F curves represent the fast and slow characteristics of the recloser and the Fuse TC and Fuse MM curves represent the total clearing and minimum melting characteristics of the fuse respectively. Notice how the curves are positioned such that devices that are further downstream have a quicker operating time. This ensures that only the device immediately upstream of a fault will operate leaving the maximum portion of the circuit energized after the disturbance has been isolated.
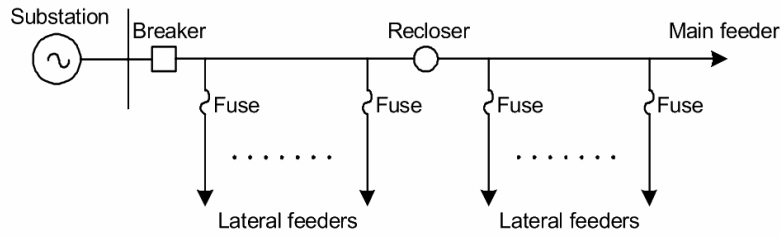
(a) Typical Distribtuion System
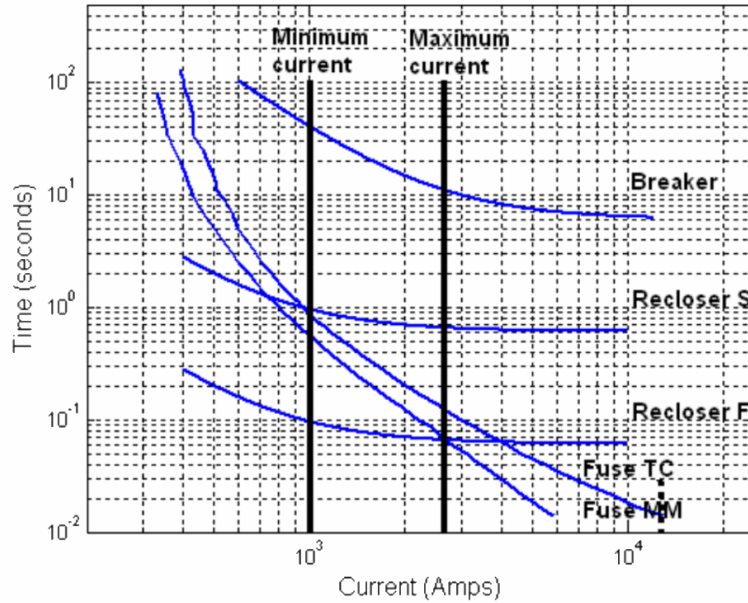
(b) TCC Curve Coordination

Figure 3.1 – Coordination of Protection Devices using TCC Curves [15]

In a reconfigured state, however, it may be true that some circuit lines or protection devices experience reverse power flow. If some type of DG were connected downstream of the recloser pictured in Figure 3.1 (a), the coordination of the recloser and breaker is no longer valid. Because of this, special consideration of the operation settings of protection devices must be considered so that misoperations do not occur. To prevent a device from operating, the current through that device should be limited to the minimum current on its TCC curve.

41

Using the BILP from Chapter Two, it is possible that the optimal solution determined by the solver causes an overloading condition of a conductor or a misoperation of a protective device. An example of this is shown in the top half of Figure 3.2.
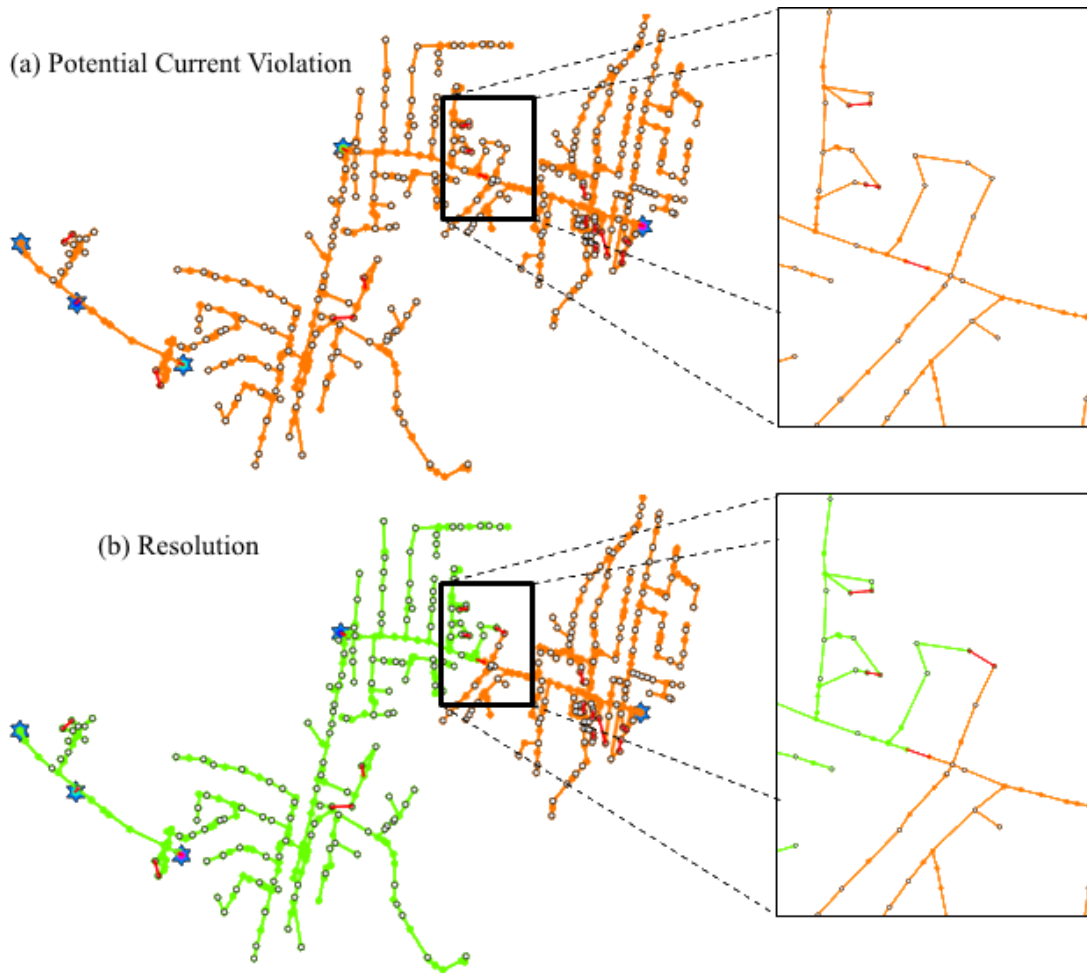
Figure 3.2 – Example of a Potential Current Violation

Here, a main line fault has occurred causing the circuit's power to be rerouted through a looped lateral section. Laterals normally do not have a large enough ampacity to carry primary current and thus this solution is not feasible. Instead, an alternative source should be closed in and the loop should remain open, as pictured in the bottom of Figure 3.2.

42

Using the ampacity ratings of conductors and operating characteristics of protection devices, the current through each edge of the graph G, representing a distribution system, can be constrained to prevent overloading. Equation (3.1) shows the general form of this constraint where I_{ij}^R is the maximum allowable current that can pass through edge (i, j).

$$-I_{ij}^R \leq I_{ij} \leq I_{ij}^R, \forall (i, j) \in E \tag{3.1}$$

Voltage constraints on a distribution system stem from the American National Standards Institute (ANSI) Standard C84.1 [16]. For residential utility services greater than 100V, the voltage supplied to the customer's meter should be within $\pm 5\%$ of the nominal service voltage. This tolerance can be separated out to the voltage drop over primary conductors and that over secondary conductors. It is recommended that less than 3% voltage drop be allowed on either so that the combined voltage drop meets the standard.

$$(1 - \epsilon)V^R \leq V_i \leq (1 + \epsilon)V^R, \forall i \in V \tag{3.2}$$

Equation (3.2) shows the constraint for voltage throughout the system where V^R is the nominal voltage and ϵ is the tolerance equal to 3% for this thesis.

Violations of the 3% recommended maximum voltage deviation may occur during reconfiguration when long circuits are tied together far from the substation. This lengthens the distance that current must travel and increase the head of feeder current of the adjacent circuit, both of which contribute to increased voltage drop. The top image in Figure 3.3 gives one such situation where a fault towards the head of Test System 2 results in a circuit tie switch being closed at the end of the feeder. The resulting voltage profile, depicted by the color contour of the circuit lines, dips towards the middle portion of the circuit and violates the 0.97 p.u. threshold in several places.

Conversely, the bottom of Figure 3.3 shows an alternative solution to the same fault scenario which does not result in voltage violations. In this solution, the circuit is tied at a different location that is more central to the loads effected by the fault.
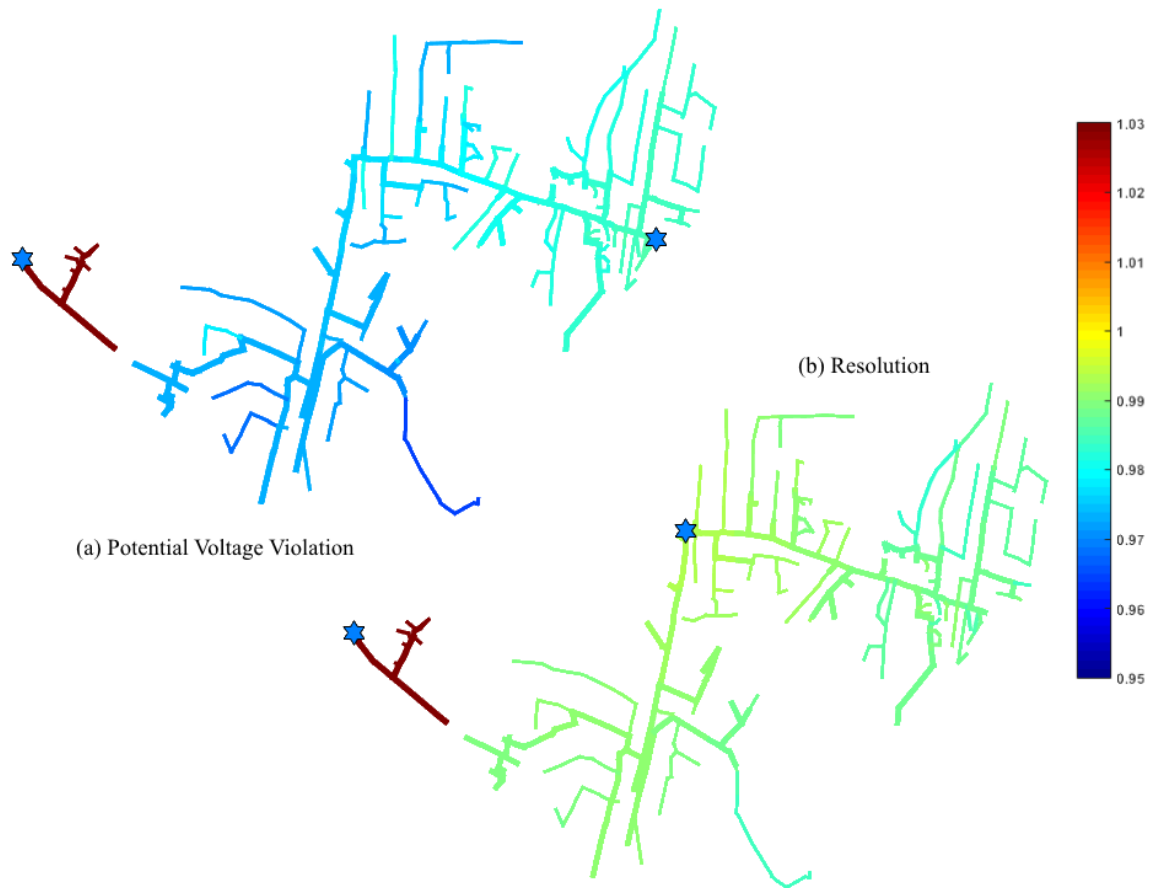
Figure 3.3 – Example of a Potential Voltage Violation

The previous two examples show that a reconfiguration scheme for distribution circuits is incomplete without considering the power flow of the reconfigured state. In the case of Figure 3.2, implementing the original solution risks damage of equipment and further compromising the system. For the example in Figure 3.3, both solutions are optimal to the reconfiguration BILP in Chapter Two because both restore power to all the loads in

the system with a single switching operation. It is much more advantageous, however, to implement the second solution so that no standards are violated and potential issues caused by under-voltage conditions are avoided.

3.3 - Linearized Power Flow Constraints

One way to validate the new configuration determined by the BILP is to do so internally. To reduce the complexity of the problem and minimize the time taken for the solver to converge, a linearized power flow model is used comparable to the DistFlow model discussed in [12].

Parameters

In addition to the parameters from Chapter Two, the following notation is used.

V^R Line to neutral reference voltage for the system. Typically $7.2kV$ or $13.8kV$ for distribution systems (corresponds to $12.47kV$ and $23.9kV$ nominal circuit voltages respectively).

ϵ Tolerance for voltage deviation limits. The National Electric Code (NEC) recommends a maximum of 3% voltage deviation for primary conductors.

ϕ_i, ϕ_{ij} The number of phases present at the vertex i and edge (i,j) respectively. Note that any edge can have, at most, the number of phases preset at its vertices: $\phi_{ij} = \min(\phi_i, \phi_j)$.

r_{ij}, x_{ij} The per-phase equivalent resistance and reactance in Ohms of the line represented by edge (i,j)

P_{ij}^R The power rating for the line represented by edge (i,j) derived from the LTE ampacity rating of the conductor multiplied by the reference voltage for the system and the number of phases. $P_{ij}^R = \phi_{ij} V^R I_{ij}^R$.

p_l, q_l Previously, p_l was defined to be the peak real power demand for the load at vertex l. In addition, q_l is the reactive power demand at peak loading conditions. Power flow will be calculated assuming that each load in the system is a constant power load meaning that p_l and q_l will not change based on the voltage at vertex l.

P_d^R, Q_d^R Similarly, both the real and reactive power ratings for each source $d \in D$ will be needed. Typically, a traditional generator will be rated so that the rated real power output can be achieved with $Q^R = \pm 0.2 P^R$, however, an inverter based source can supply the full rated power in VARs, $Q^R = P^R$.

Variables

The two key power flow results that will be used to enforce the power flow constraints are the voltage at each vertex and the power flowing through each edge. Thus, new variables will be needed to denote these values.

$V_i \in \mathbb{R}$ $\forall i \in V$ Magnitude of the Voltage at vertex i

$P_{ij}, Q_{ij} \in \mathbb{R}$ $\forall (i,j) \in E$ Real and reactive power flowing through edge (i,j)

$s_{ij} \in \mathbb{R}$ $\forall (i,j) \in E$ Slack Variable for voltage difference between vertices i and j when section $(i,j) \in G^0$

$P_d, Q_d \in \mathbb{R}$ $\forall d \in D$ Real and reactive power supplied from source i

Assumptions

The assumptions made in Chapter Two about each source having the ability to be dispatched and each section being able to be switched should also be made for this formulation. Additionally, simplification of the power flow model will require three major assumptions.

First, all loads are modeled as constant power loads with a constant real and reactive demand. This allows for the power flow to be solved as a network flow problem since the "sink" nodes will not be dependent on the voltage. Second, voltage drop will be calculated using a decoupled single phase equivalent resistance and reactance for the conductors. Calculating in this way will typically overestimate the voltage drop ensuring that the actual system will stay within the limits while using less computational power. Finally, all sources are assumed to have a scheduled voltage, providing a reference point for the voltage drop calculations. Typically, when a source is dispatched, it will have a set voltage output, however this assumption is not entirely accurate for circuit tie locations. To adjust for this, a power flow is calculated before reconfiguration and the pre-disturbance voltage at each circuit tie location is used as the voltage reference for that source.

Constraints

The first two constraints defined in equations (3.3) and (3.4), set up the network flow problem used to approximate the power flow. Comparable to Kirchhoff's Current Law (KCL), the power flowing into each vertex is set to equal the power leaving.

$$\sum_{(j,i)\in E} P_{ji} + \sum_{i\in D} P_i = \sum_{(i,j)\in E} P_{ij} + \sum_{i\in L} \sum_{k=1}^{|D|} A_i^k p_i \, , \forall i \in V \qquad (3.3)$$

$$\sum_{(j,i)\in E} Q_{ji} + \sum_{i\in D} Q_i = \sum_{(i,j)\in E} Q_{ij} + \sum_{i\in L} \sum_{k=1}^{|D|} A_i^k q_i \, , \forall i \in V \qquad (3.4)$$

A side effect of computing the power flow in this manner is that the losses over each edge are neglected. Note that the power flow variable P_{ij} is defined in such a way that it measures the power flowing from vertex i to vertex j. Power may end up flowing in the opposite direction in which case P_{ij} will be negative.

Next, the voltage drop across each edge is estimated. The following shows the voltage drop between vertices i and j calculated as a function of the power flowing through edge (i,j) and the voltage at vertex j. Note that the voltages here are phasor values.

$$\widetilde{V_i} - \widetilde{V_j} = \widetilde{I_{ij}}\widetilde{Z_{ij}} = \left(\frac{P_{ij}+jQ_{ij}}{\phi_{ij}\widetilde{V_j}}\right)^* (r_{ij} + jx_{ij}) = \frac{P_{ij}r_{ij}+Q_{ij}x_{ij}+j(P_{ij}x_{ij}-Q_{ij}r_{ij})}{\phi_{ij}\widetilde{V_j}}$$

Since the voltage angels are small, the imaginary portion of the voltages can be neglected. In addition, the receiving end voltage is approximated using base voltage of the system, resulting in equation (3.5). Here s_{ij} is used as a slack variable, constrained in (3.6), and M is sufficiently large enough to relax (3.5) when edge (i,j) is inactive ($b_{ij}^0 = 1$).

$$V_j = V_i - \frac{P_{ij}r_{ij}+Q_{ij}x_{ij}}{\phi_{ij}V^R} + s_{ij}, \forall(i,j) \in E \tag{3.5}$$

$$-b_{ij}^0 M \leq s_{ij} \leq b_{ij}^0 M \tag{3.6}$$

With the power flow and voltage drop relationships constrained, the bounds on voltage at each vertex and power flowing in each edge can be established. First, the voltage is required to remain within some tolerance ϵ of the nominal voltage of the system.

$$V^R(1 - \epsilon)(1 - a_i^0) \leq V_i \leq V^R(1 + \epsilon)(1 - a_i^0), \forall i \in V \tag{3.7}$$

Likewise, each conductor should not carry more power than its rating will allow or carry no power when the edge is inactive. The power ratings used for each edge are derived from the conductor LTE ampacity and the rated system voltage described previously. No more

than 20% of the conductor ampacity should be used for reactive power flow. Inequalities (3.8) and (3.9) enforce these conditions using b^0 to indicate if the edge is inactive.

$$-P_{ij}^R\left(1 - b_{ij}^0\right) \le P_{ij} \le P_{ij}^R\left(1 - b_{ij}^0\right), \forall (i,j) \in E \tag{3.8}$$

$$-0.2P_{ij}^R\left(1 - b_{ij}^0\right) \le Q_{ij} \le 0.2P_{ij}^R\left(1 - b_{ij}^0\right), \forall (i,j) \in E \tag{3.9}$$

Finally, the capacity of each source must not be exceeded or the power from the source must be zero when it is inactive. Inequalities (3.10) and (3.11) use the rated real and reactive power for each source and the variable A to enforce this constraint.

$$P_d \le \sum_{k=1}^{|D|} A_d^k P_d^R, \forall d \in D \tag{3.10}$$

$$Q_d \le \sum_{k=1}^{|D|} A_d^k Q_d^R, \forall d \in D \tag{3.11}$$

This is like constraint (2.13) from Chapter Two which prevented a subgraph from supplying more load than the capacity of the connected sources. In fact, using the above equations results in (2.13) becoming redundant, thus it is removed from the formulation.

Results and Discussion

Test Systems 1 and 2 are used in this chapter to test the partitioning method with linearized power flow constraints enforced internally. For more information on these two test systems, please refer to Section 2.5 and Figure 2.3.

OpenDSS is an open source simulation tool developed by the Electric Power Research Institute (EPRI) that is designed specifically for the modernizing distribution grid. The simulator is particularly good for calculating steady-state power flows and can be controlled through a COMM interface by several different programming interfaces

including Matlab. For this chapter, OpenDSS is used to compare with the power flow estimates calculated in the LP for the various system configurations.

Test System 1

The load composition for the Test System 1 is highly inductive, composed of an aggregate total of 4.66 MVA at a power factor of 0.8159 at peak. In addition, the circuit does not contain any capacitors. Recall that, to linearize the voltage drop calculation, the imaginary part of the voltage drop was ignored. This means that more reactive power flowing in the circuit will cause a greater disparity between the linearized estimate and the actual voltage drop. Consequently, the circuit is tested at 50% peak real power and 30% peak reactive power, increasing the power factor of the aggregate load to 0.9201.

For the first test case, the system configuration is determined under normal operation and the resulting voltage profile is compared to a full power flow calculated using OpenDSS, pictured in Figure 3.4.

(a) OpenDSS Power Flow Results   (b) MILP Power Flow Results
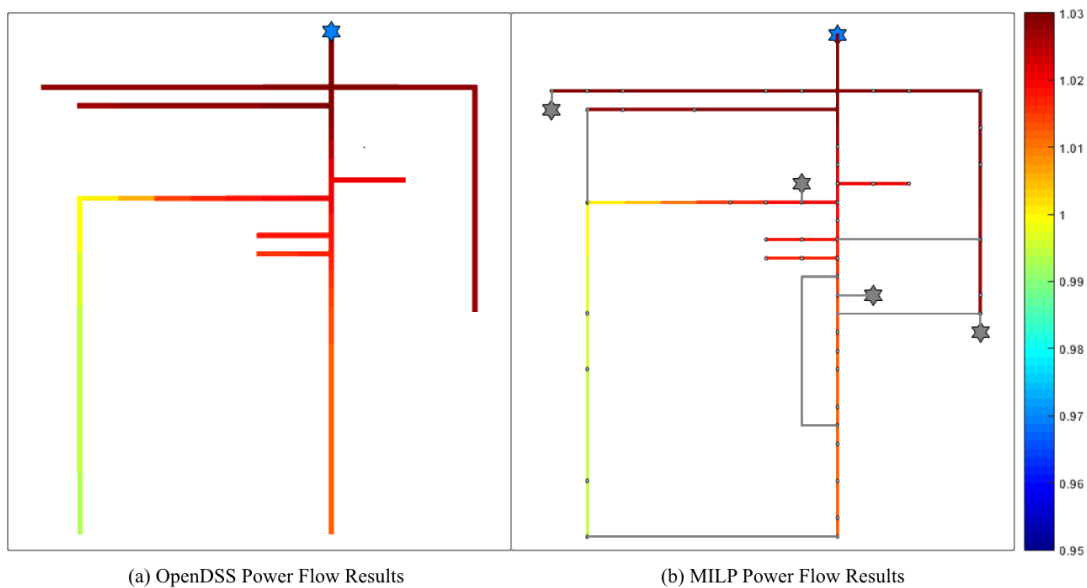
Figure 3.4 – MILP Results for Test System 1 during Normal Operation

Test System 1 is a balanced three-phase circuit and the line resistances and reactance are given as sequence components. A power flow calculation on this type of circuit is comparable to the simplified power flow used in this section. Thus, the voltage profiles from each computation are similar with the MILP voltages being slightly lower. The minimum voltage achieved in the circuit is 0.994 p.u. which is well above the 3% voltage drop limit. This test case shows that the method configures the system correctly for the trivial case and that the approximations made in the power flow calculations do not have a large effect on the power flow results for this system at these loading conditions.

Next, the multiple main-line fault scenario was simulated for the test system and the optimal configuration was found subject to the power flow constraints.

(a) OpenDSS Power Flow Results   (b) MILP Power Flow Results
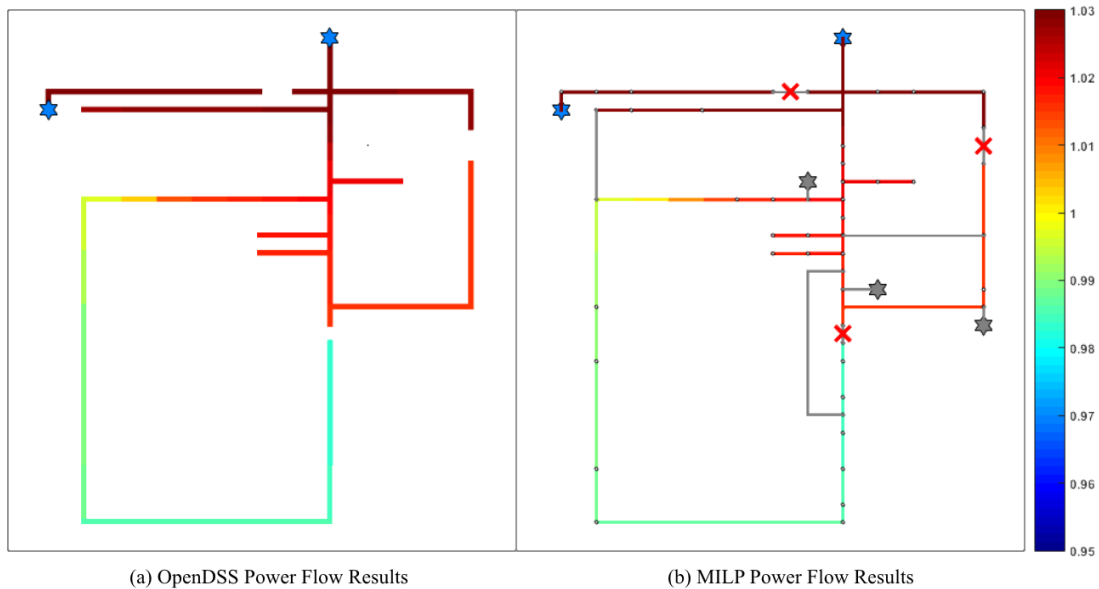
Figure 3.5 – MILP Results for Test System 1 during Faulted Operation

The results, shown in Figure 3.5, vary slightly from the results generated in Chapter Two from the same scenario (Figure 2.4). This variation, however, is not due to the power flow

51

constraints as both solutions are feasible and optimal in both formulations. Rather, the CPLEX solver does not check for multiple optimal solutions, but returns the first optimal solution that is found. In this case, the solution closing the alterative tie switch was simply found before the previous solution given.

Comparing the voltage profile resulting from OpenDSS (left) to the voltage profile from the MILP (right) in Figure 3.5, it can again be seen that the linearization had a negligible effect. The MILP again generated a comparable voltage profile to OpenDSS, returning slightly lower voltages with the minimum voltage being 0.984 p.u. It is also important to note that no current violations were found after running the OpenDSS power flow indicating that the overloading constraint in the MILP is working properly.

Test System 2

Unlike the IEEE 69-Bus System, Test System 2 is an unbalanced three phase model complete with wire data, line spacing information, and cable data for each section of conductor. This allows for a true unbalanced power flow to be calculated and compared with the linearized model. The total aggregate peak load of the system is 7.48 MVA at a power factor of 0.9603 (including two capacitors totaling 900 kVAR). Since the power factor of the load is relatively close to unity, 100% peak real and reactive power was used to formulate the power flow constraints for Test System 2.

Under normal system operation, the disparity in voltage profile is much more pronounced for Test System 2 than Test System 1 indicated by the color differences in Figure 3.6.The minimum voltage achieved from the MILP was 0.982 p.u. compared to 0.994 from the unbalanced power flow calculated in OpenDSS. Despite the inaccuracies

caused by the decoupled linearized power flow, these results show that the MILP over estimates the voltage drop and can provide a solution that does not contain any voltage violations.
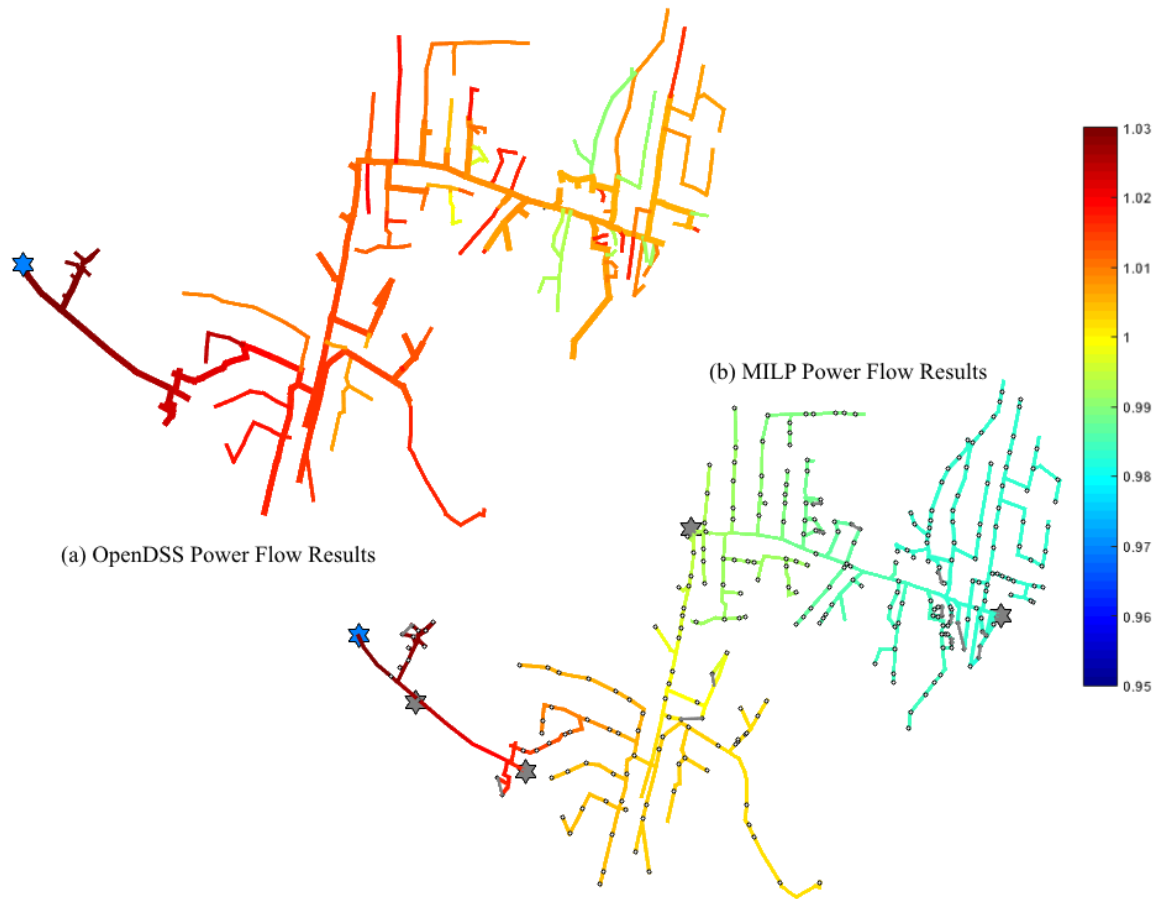
Figure 3.6 – MILP Results for Test System 2 during Normal Operation

Comparison with Previous Formulation

As expected, the solve time for all cases discussed increased with the addition of the power flow constraints. Table 3.2 shows the convergence information for each test case. Most notable are the time increases in the faulted operation of Test System 1 and the normal operation of Test System 2 which saw an increase in convergence time of 15 times and 10

times respectively. The longer solution times can be attributed to the additional variables and constraints that are required for the power flow constraints. For the IEEE 69-Bus test system, a total of 326 variables and 874 constraints are added by the power flow formulation bringing the totals to 1612 and 2297 respectively. Similarly, the Suburban Distribution Circuit had variable and constraint increases of 2749 and bringing the totals to 13440 and 18952 respectively.

Table 3.2 – Linearized Power Flow Constraints Convergence Results

Test Case	Converged	Relative Gap	Solution Time
Test System 1 - Normal Operation	Int. Optimal	0	0.7040 s.
Test System 1 - Faulted Operation	Int. Optimal	0	4.5684 s.
Test System 2 - Normal Operation	Int. Optimal	0	23.87 min.

While the solution times for Test System 1 remained reasonable, the result for Test System 2 is too long for real time implementation. To account for this in the previous chapter, system reduction was used, however, the same method cannot be applied in this case. Collapsing adjacent sections into a single node would change the electrical properties of the system, affecting the power flow results. A reduction technique could be formulated that has minimal effect on the electrical properties of the system, however, such a reduction technique would be much more complicated and is not presented in this thesis.

3.4 - Two-Step Method

Another method for enforcing power flow constraints on the BILP from Chapter Two is to simply calculate a power flow after the solution is found and check for violations. This allows for software that is built specifically for unbalanced, three-phase power flows, to be used that can better estimate the conditions of the system after switching has occurred.

Figure 3.7 shows how this two-step method of first partitioning the network and then validating the power flow, is implemented in a closed loop algorithm to find solutions that satisfy the overloading and voltage variation constraints for the circuit.
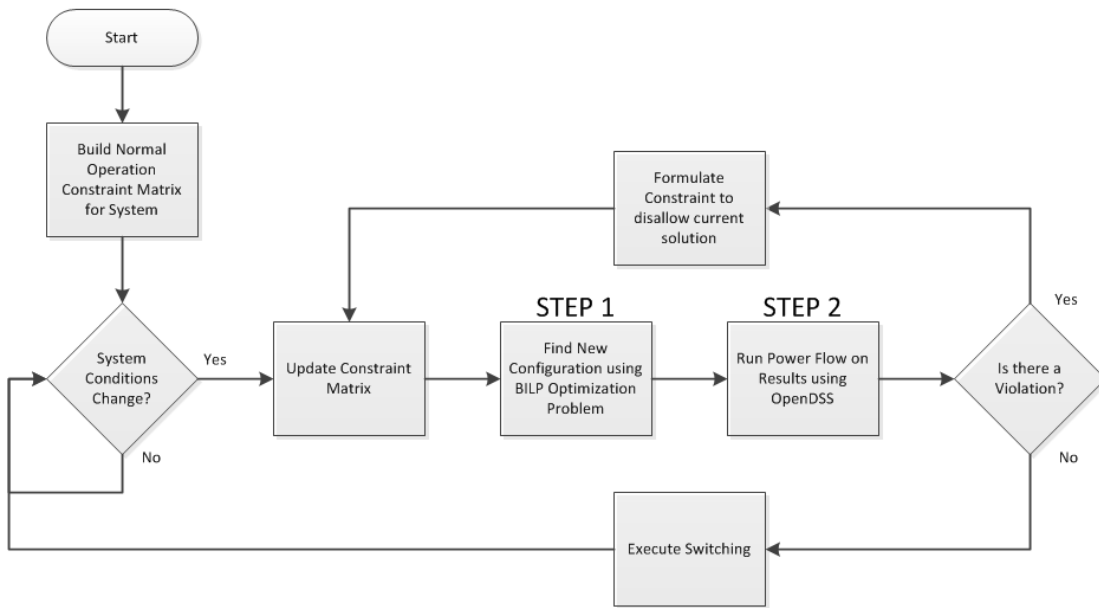
Figure 3.7 – Two-Step Method for Power Flow Constraint Validation

For the method to work, a constraint must be formulated and added to the BILP that will prevent the solver from obtaining a previous solution after a violation has been detected. As shown previously the optimal solution of the BILP is not necessarily unique and, in

fact, it is guaranteed to not be unique. This is because simply relabeling the active subgraphs of any feasible solution would result in another feasible solution that has the same objective function value. Since the numbering of subgraphs is arbitrary, however, all solutions which partition the graph in the same way but label it differently are effectively equivalent so this does not misrepresent the problem.

On the other hand, changing the switching results of the solution does result in a different solution. Thus, the variable B, which indicates if a switch has operated or not, is used to enforce this constraint. Inequality (3.12) requires at least one B_{ij} to change from the previous solution B^{k-1} which prevents the solver from returning the same partition as the previous iteration while still allowing any other combination of switching operations.

$$\sum_{B_{ij}^{k-1}=1} B_{ij}^k + \sum_{B_{ij}^{k-1}=0}\left(1 - B_{ij}^k\right) \leq |E| - 1 \tag{3.12}$$

Note that if $B^k = B^{k-1}$, the left side of the inequality equals $|E|$ and the constraint is violated. Implementing this method allows for the same system reduction used in Chapter Two to be applied while simultaneously providing a way to prevent violations in the reconfigured state found by the BILP. Once the optimal partition is found, the solution is simply mapped back to the original system. OpenDSS is then used to solve for an unbalanced power flow and check for overloading and voltage violations.

Results and Discussion

The reduced models of Test Systems 2 and 3 are used in this section to test the two-step partitioning method for enforcing power flow constraints. For more information on these two test systems, please refer to Section 2.5 -, Figure 2.6, and Figure 2.8.

Test System 2

To test the two step method, three random fault locations where applied to Test System 2 until a scenario was found that required multiple iterations to return a solution without violations. Many scenarios tested found solutions without violations on the first iteration, however, the scenario shown in Figure 3.8 was eventually found. This scenario is like the example given earlier in this chapter in Figure 3.3 where a fault that is near the head of the feeder has occurred, isolating most of the circuit from the substation. When solved initially, an upstream source was connected to energize the downstream sections.
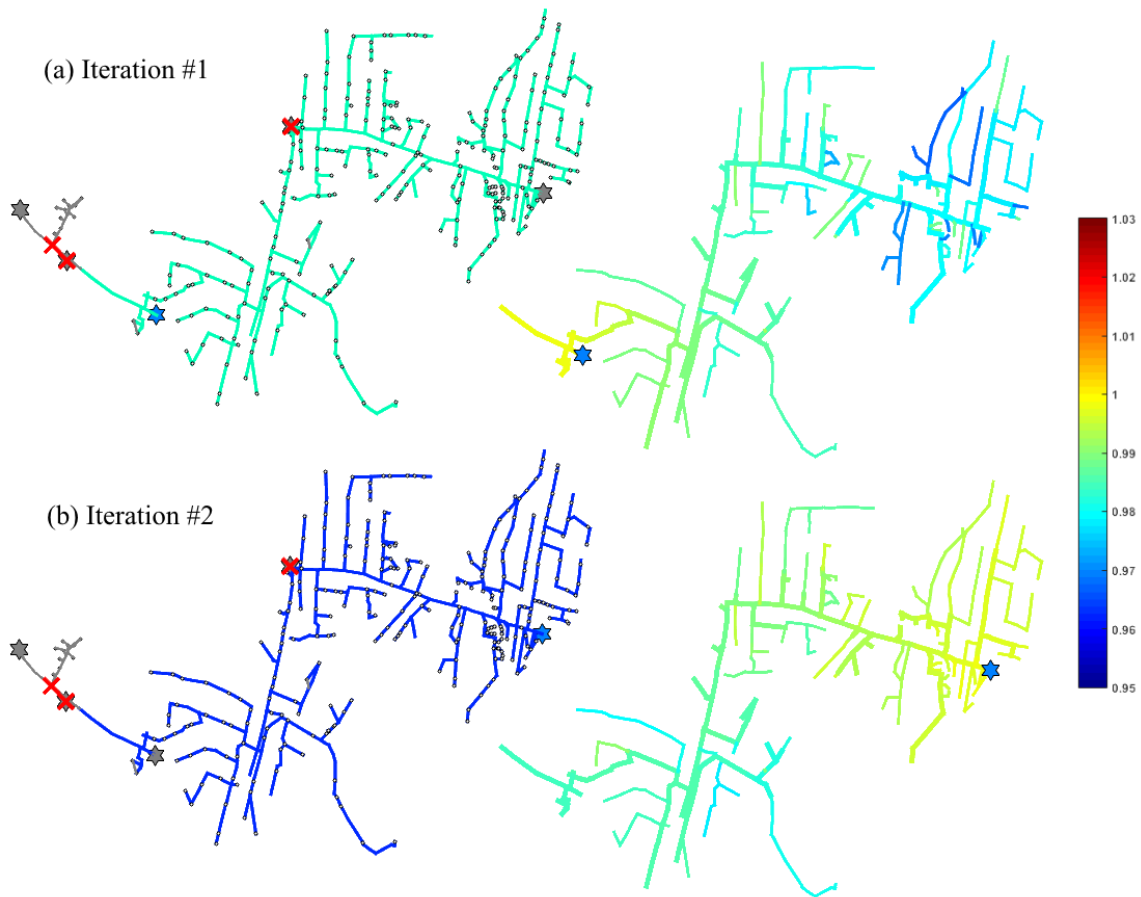
Figure 3.8 – Two-Step Method Results for Test System 2 during Faulted Operation

As shown in the top part of Figure 3.8, however, this causes voltage violations towards the end of the feeder. Once inequality (3.12) was added to the constraint matrix and the problem was solved again, the source towards the end of the feeder was chosen to energize the circuit. Since this source is more closely located to the load center, less voltage drop over the lines occur and no violations were found.

Test System 3

Similarly, the Two-Step Method was applied to Test System 3 both at normal operation and faulted operation. Figure 3.9 shows the results during normal operation.
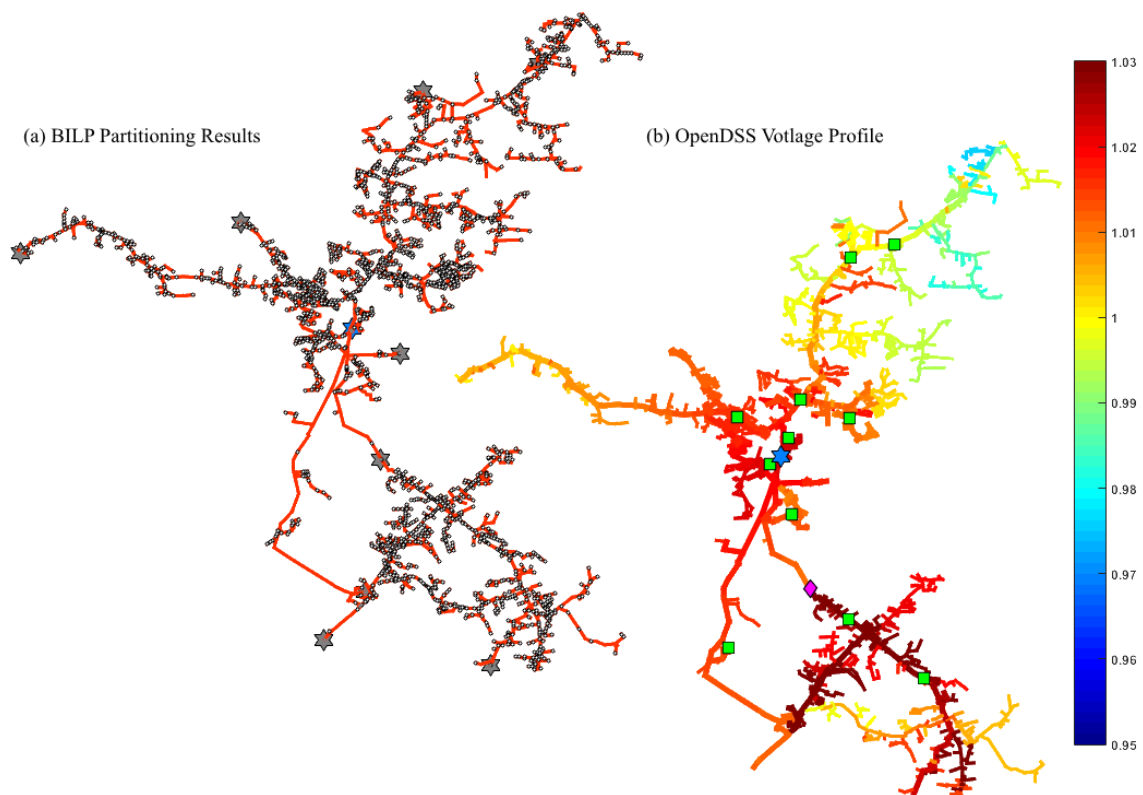
Figure 3.9 – Two-Step Method Results for Test System 3 during Normal Operation

One of the major benefits of using the Two-Step Method over the linearized power-flow constraints is that more complicated circuit elements with control schemes such as voltage regulators and switched capacitors can be considered by the power flow. Test System 3 has a voltage regulator in the bottom part of the circuit marked by the purple diamond in Figure 3.9. If this voltage regulator were neglected, the circuit voltages calculated downstream would most likely fall outside the 3% threshold and the normal operation of the circuit would not be feasible. With the Two-Step Method, however, this is not an issue and the proper system configuration is found at normal operation.

Finally, the Two-Step Method applied to a faulted scenario on Test System 3 is shown in Figure 3.10 on the following page. As with Test System 2, random fault scenarios were placed on the system until one resulted in multiple iterations. Notice the low voltages in the bottom part of the feeder in the first two iterations (a) and (b). This is due to the back-feeding condition that the regulator, not marked in the figure, experiences in these configuration. Once the source upstream of the regulator is connected, the device can operate properly and adjusts the voltage in this section of the circuit above the threshold shown in part (c) of the Figure 3.9.

Back-feeding of a voltage regulator is a dangerous system condition and can have undesirable effects on the distribution system. In fact, utilities will typically not connect any DG downstream of a voltage regulator to prevent this condition. The BILP from chapter 2 is blind to the fact that voltage regulation exists on this circuit and thus it is imperative that the power flow be calculated and checked for violations such as these before switching can occur.

(a) Iteration #1

(b) Iteration #2

(c) Iteration #3
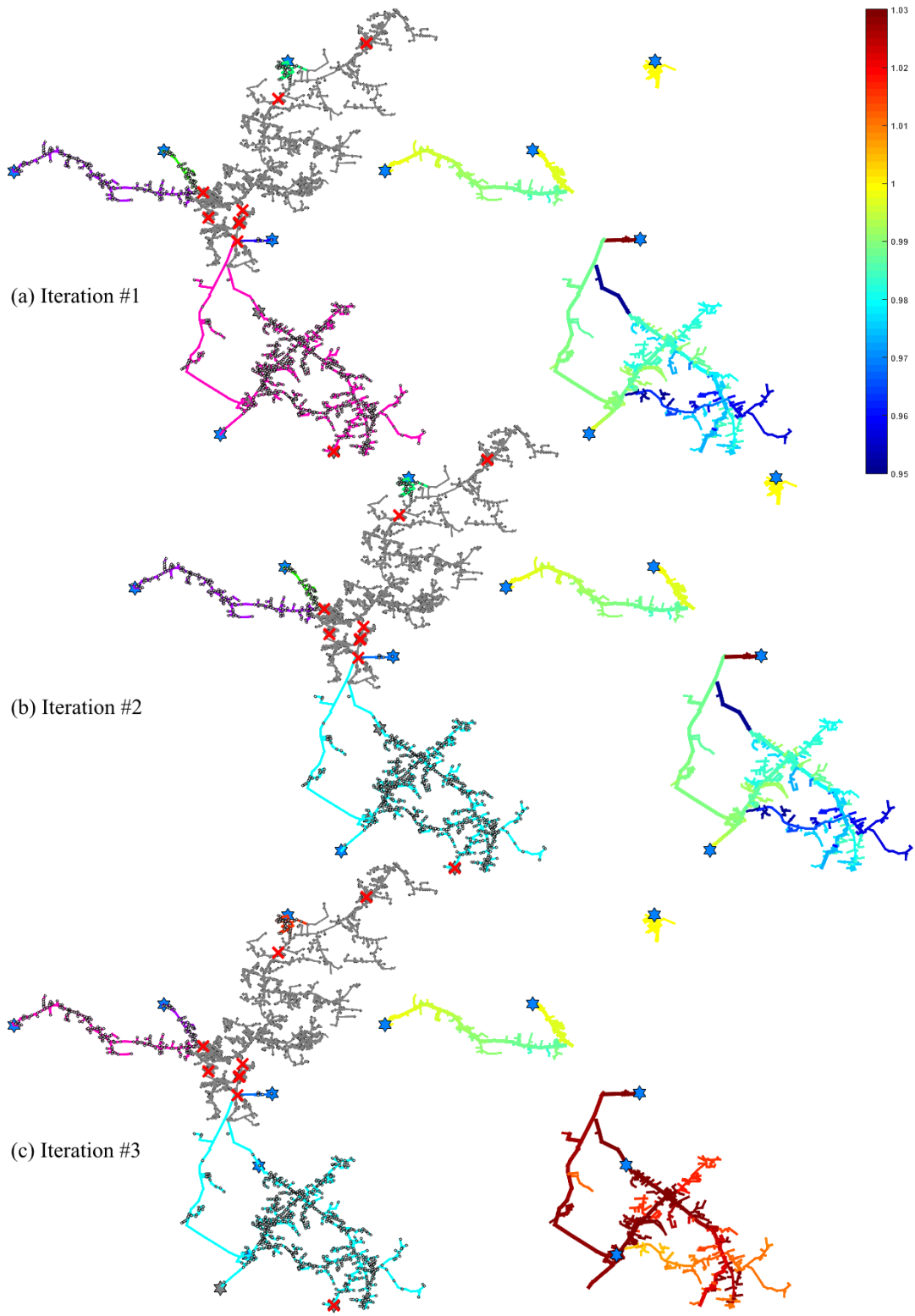
Figure 3.10 – Two-Step Method Results for Test System 3 during Faulted Operation

Comparison with Previous Formulation

Since the Two-Step Method allows for model reduction in the same way that it was used in Chapter Two, the solution times are comparable. Table 3.3, shows the convergences times divided up by each of the two steps. It should be noted that the power flow calculation time also includes the time required to map the solution of the BILP back to the original graph, initialize OpenDSS, compute the power flow, and check for violations whereas the BILP Solution Time is only the time used by the CPLEX solver to converge.

Table 3.3 – Two-Step Method Convergence Results

Test Case	Iterations	BILP Solution Time	Power Flow Calc. Time
Test System 2 – Faulted	2	0.1477 s.	0.2439 s.
Test System 3 - Normal	1	0.1572 s.	0.9736 s.
Test System 3 - Faulted	3	4.7294 s.	6.2658 s.

For larger systems, the key to finding solutions to the reconfiguration problem is model reduction. The significant difference between the linearized power flow method and this method is that a simple model reduction can still be used and the results confirm the importance of model reduction. All the solution times in the table are sufficiently quick and even for the scenario requiring three iterations of the Two-Step Method, requiring a total time of 10.98 s, the solutions are fast enough for the method to reconfigure a circuit in real time.

3.5 - Conclusion

Chapter Three has explored methods to check reconfiguration circuits for violations including conductor overloading and under voltage. The first method used a linearized power flow calculation to constrain the power flowing through each edge and the voltage deviation at each vertex in the distribution system graph G. These constraints were enforced in test scenarios on two test systems and were shown to perform desirably in both the trivial case, normal operation, and the multiple main line faulted case. When compared to the original formulation, it was noted that the power flow computation greatly increases the solve time of the LP. In addition, this result is magnified for larger test systems.

The second method discussed is an iterative one that calculates a power flow externally to the LP and uses a feedback loop to recalculate the solution if a violation is found. This method was shown to perform favorably to the linearized constraints in several ways. First, using programs like OpenDSS allows for the unbalanced power flow calculated outside of the LP to account for complicated control schemes for elements like voltage regulators and switched capacitors without adding much computational time. This is better than the linearized constraints because it can provide a more accurate estimate of the post-reconfiguration conditions on the circuit and is more universal in that it can accommodate more systems. Secondly, the Two-Step Method allows for the use of model reduction. This is a great benefit for larger systems as the number of edges and vertices has a great impact on the convergence time of the problem.

CHAPTER FOUR

OPTIMAL LOCATION OF BATTERY ENERGY STORAGE ADAPTED FROM THE

CAPACITOR PLACEMENT PROBLEM

4.1 - Introduction

Inverter-based Battery Energy Storage Systems (BESS) are widely thought to provide a solution for many of the issues caused by the variability of Distributed Generation (DG), specifically Photovoltaic (PV) generation. As a result, there is a great deal of focus in academia to study different aspects of BESS integration into the grid. Sizing of batteries [17, 18] and optimal control of batteries [19, 20] are often considered, but one research topic that is somewhat neglected is the optimal location of a BESS on a distribution feeder. This is because it is often assumed that it is optimal to place the BESS at the point of common connection (PCC) with the grid. This problem becomes more complex, however, when multiple large scale DGs are considered or in the event of residential DG spread throughout a circuit.

Furthermore, a battery can add value in a number of other ways not related to DG mitigation. Examples of this can vary from reducing voltage flicker, reducing the thermal loading on upstream conductors and preventing the need for conductor replacement, providing a redundant power source for critical loads during outage situations, and in the case of smart inverters, contributing to the reduction of losses by providing a demand side management tool and reactive power support. This chapter will explore the hypothesis that there is value in locating a BESS such that the battery's ability to affect a distribution circuit by providing real and reactive power support and reduce losses is maximized.

When treating a BESS as a loss reduction asset, the optimal location problem becomes similar to the Optimal Capacitor Placement (OCP) problem. Therefore, in order to explore a BESS's ability to reduce losses, an OCP approach will first be developed and tested. Once validated, the strategy for locating capacitors will then be generalized for a BESS which can consume or supply both real and reactive power. The results of this chapter will show the effect that the placement of the BESS has on the power losses in a distribution circuit with various levels of PV penetration.

4.2 - Background Information

Reactive power occurs due to the phase shift between voltage and current across inductive or capacitive loads. In the case of inductive loads, the current has a lagging response to the voltage meaning that the zero crossing of the current waveform occurs after that of the voltage waveform. Capacitors have the opposite effect, causing the current waveform to lead the voltage waveform. The effect of this is that the load receives power during half of the cycle that it then provides back to the source during the other half, resulting in a zero-net exchange of energy. Often called "imaginary" power, the exchange between load and source requires extra current to flow in the lines that connect the two. For a distribution system, this means extra losses in those lines as well. Placing capacitors on distribution systems can have the desired effect of reducing these losses by offsetting the phase shift caused by inductive loads on the system.

Existing Approaches to Capacitor Location and Sizing

Location and sizing are the two keys to a capacitor effectively reducing losses. It is often beneficial to think of a capacitor as a "reactive power source" that supplies the

inductive loads on the system. If this capacitor is located far away from those loads or is inappropriately sized, the effect on reducing losses can be minimal or in some cases, losses can even increase.

The simplest method for locating capacitors on a circuit with a uniformly distributed load, is called the 2/3's rule [21]. This rule states that the optimal size and location for a capacitor is 2/3's of the circuit's reactive power and 2/3's of the way down the feeder respectively. Pictured in Figure 4.1 is an illustration of the 2/3's rule for a feeder with 3 MVARs of reactive power demand.
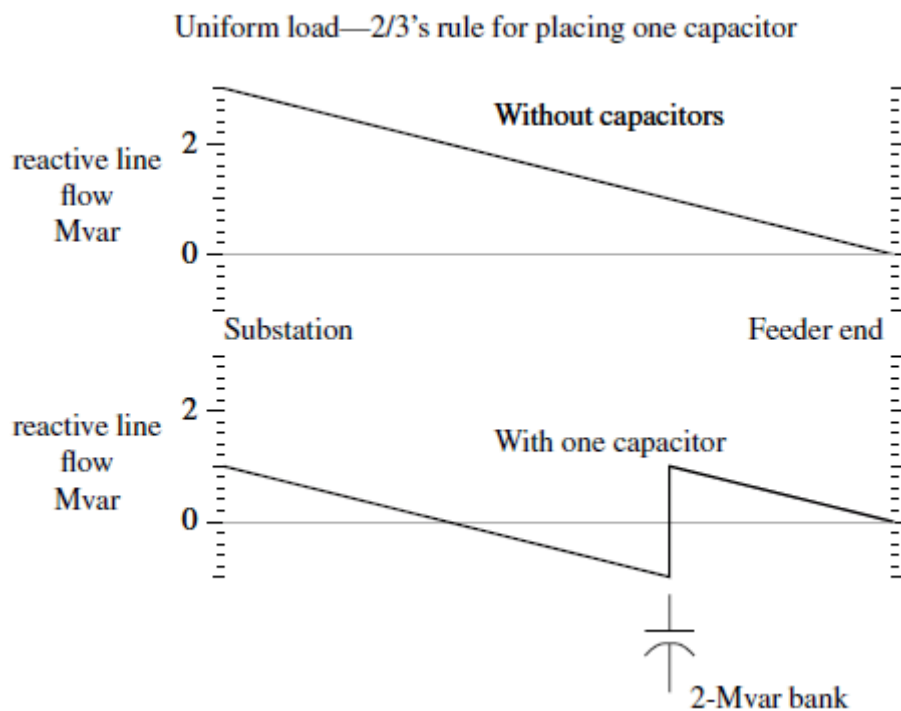
Figure 4.1 – Capacitor Location using 2/3's Rule

Notice that the optimal location is the one that results in the minimal area between the x-axis and the reactive power profile and actually results in "negative" reactive power

for a portion of the feeder. The negative MVAR signifies sections of the circuit where the current is leading the voltage, and can be interpreted as reactive power flowing in reverse; i.e. from the capacitor toward the source. Another important idea from Figure 4.1 is that the reactive power flow is only changed in the lines upstream of the device. This further demonstrates the importance of locating a capacitor correctly.

Sizing can often be thought of as a separate problem to be solved before location is considered. Many times utilities will add a specific amount of capacitance to a circuit to achieve a certain power factor at the head of the feeder, known as power factor correction. However, reactive power demand may change with the time of day or season requiring the use of switched or variable capacitors. Figure 4.2 is a plot of monthly average reactive load-duration curves from a 2014 data set received from a local utility.
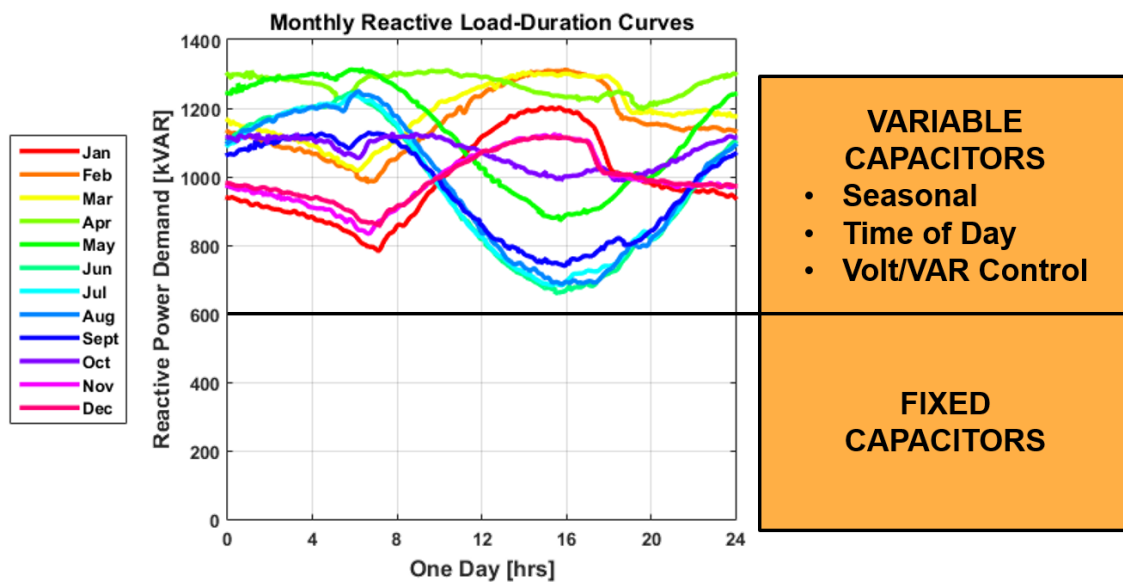
Figure 4.2 – Monthly Average Reactive Load-Duration Curves

This data set contains head of feeder measurements for a rural distribution circuit over an entire year at 1 min. resolution including voltage, current, real power, and reactive power. The kVAR from two capacitors located on the circuit were added to the reactive power measurements (switched capacitor operations were determined from sudden changes in the head of feeder reactive power measurements), and the days from each month were averaged together. This circuit contains a 600 kVAR fixed capacitor and a 450 kVAR switched capacitor which are reasonable selections based on the figure.

Utilities often prefer rule-based methods for sizing and locating capacitors due to their simplicity and the ease by which they can be implemented. The Grainger/Lee Method (1981) is an extension of the 2/3's rule for locating multiple capacitors on a single system that is popular among utilities [22]. More complicated approaches include Loss Sensitivity Analysis [23], the study of how sensitive one parameter, in this case losses, is to changes in other parameters, and Particle Swarm Optimization [24], a popular stochastic optimization method developed in 1995 similar to genetic algorithms. The method chosen for this thesis is Mixed Integer Programming (MIP).

4.3 - Optimal Capacitor Placement Formulation

Let the distribution system again be represented by the graph $G = (V, E)$, defined in Chapter Two, where each vertex $v \in V$ corresponds to a power distribution pole or pad mount location and the edges $e \in E$ represent the conductors or cables that connect them.

$$V := \{1, \dots, N\} \qquad E := \{(i, j)\} \subset V \times V$$

Additionally, the set C is used to identify the vertices in V that have an existing capacitor.

$$C := \{c \in V : an\ existing\ capacitor\ is\ connected\ at\ vertex\ c\}$$

For this formulation, it will be assumed that only one capacitor will be located at a time. If multiple capacitors are to be added to the system, they can be optimized one by one with each location being added to C after the preceding solution has been found.

Characterizing a Feeder's Demand

To optimize the placement of any demand side management asset, an understanding of the demand that exists on the feeder in question must first be obtained. Figure 4.3 shows a two-dimensional histogram of a circuit's real and reactive power demand plotted from the same data set discussed in Figure 4.2. The histogram separates real and reactive power conditions into a 20×20 grid and counts the number of times a measurement falls within each square, or bin, in the grid. These results are then normalized by the total number of data points collected over the entire year and plotted as a bar along the vertical axis.
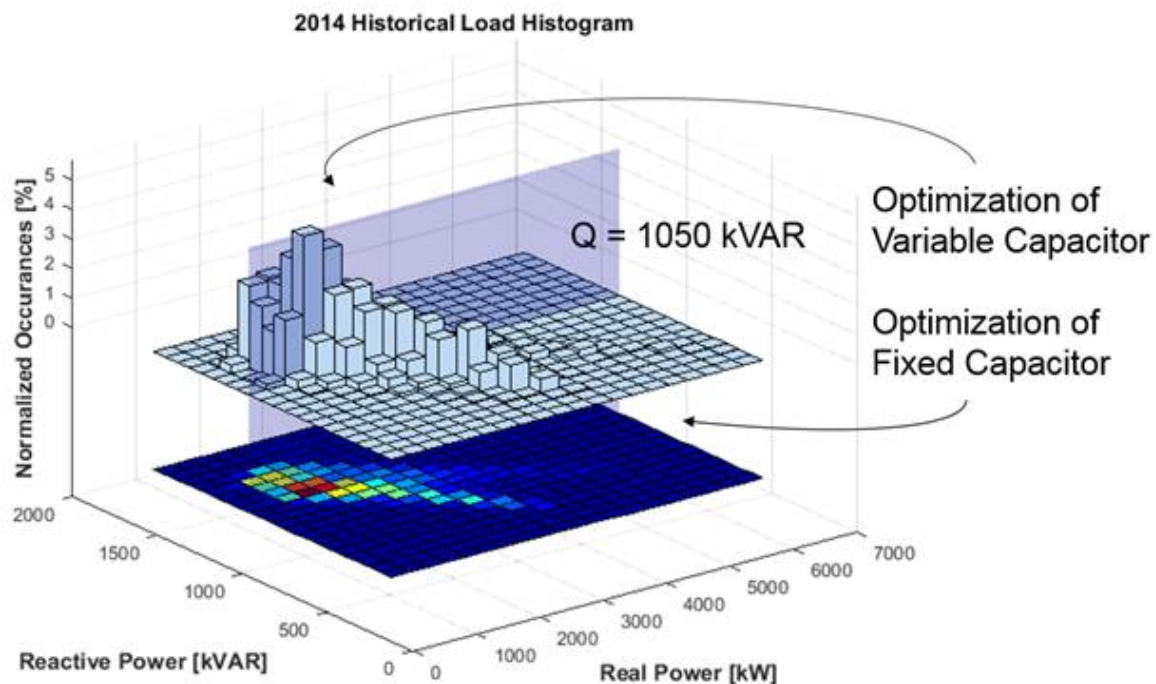
Figure 4.3 – Two-Dimensional Histogram of 2014 Real and Reactive Demand

As indicated in the figure, the fixed capacitor will be optimized over the set of points where the variable capacitor with be turned off. For this circuit, this is when the reactive power demand is less than 1050 kVAR (sum of the ratings of the two capacitors on the circuit). The variable capacitor should be optimized over the remaining data and with the fixed capacitor already added to the circuit.

Maximizing the benefit of a capacitor means ensuring that it operates optimally during the average loading conditions on the circuit. This means that outliers, or conditions that do not occur often, can be ignored. By removing less than 0.5% of the data, the 191 non-empty bins is reduced to 110 for the given circuit data. Let the set M contain labels that create a map to each of the non-empty bins in the histogram excluding outliers.

$$M = \{m : m \rightarrow (P_m, Q_m)\}$$

This will allow the effect of the capacitor to be averaged over the wide variety of loading conditions that the circuit will experience throughout a year.

Parameters

The following notation is used to define the parameters given in the problem.

V^R Line to neutral reference voltage for the system, typically, $7.2kV$ or $13.8kV$ for distribution systems.

Q_c^R Three-phase reactive power rating in kVAR for the capacitor at vertex c.

Q_{new}^R Three-phase reactive power rating in kVAR for the new capacitor that will be located by the problem.

p_l, q_l Real and reactive power demand for the load at vertex l defined at peak conditions.

β_p^m, β_q^m Multipliers for load level m where $0 \leq \beta \leq 1$. β represents the percentage

of peak real and reactive power demand that the distribution system is

experiencing during m. These multipliers are the values on the x and y-axis

of Figure 4.3 normalized by the peak demand at which p and q are defined.

w^m Normalized weights for load level m. These weights are the corresponding

z-value for each bin in Figure 4.3 representing the percentage of the year

that the loading conditions represented by m occur.

r_{ij} The per-phase resistance in Ω's of the conductor represented by edge (i, j).

Variables

The following notation will be used to define the variables that are minimized over.

$$C_i \in \{0,1\} \quad \forall i \in V \quad = \begin{cases} 1 & \text{New capacitor is located at node } i \\ 0 & o.w. \end{cases}$$

$P_{ij}^m, Q_{ij}^m \in \mathbb{R} \quad \forall (i, j) \in E, m \in M$ Real and reactive power flowing through

edge (i, j) for each load level m.

Assumptions

The same assumptions made for the linearized power flow constraints in Chapter

Three will be made for the power flow calculated in this problem. All loads are considered

to be constant power loads and the losses are calculated per-phase assuming the positive

sequence and mutual coupling are equal between phases. Furthermore, the effects of DG

are not considered by the OCP problem. The goal of developing this problem is to compare

the results to existing capacitor locations. Most existing capacitors pre-date the installation

of DG and thus did not influence their placement.

Objective Function

The goal of the OCP problem is to minimize the average $|I|^2R$ losses for the system over the entire year. To do this, a separate power flow is calculated for each unique loading condition in M. Using this power flow, the objective function should sum up all the losses. Below is a derivation showing the value of $|I|^2$ in terms of the variables P and Q, where the reference voltage for the system V^R is used to approximate the receiving end voltage V_j.

$$|I_{ij}|^2 = \left|\frac{S_{ij}}{3V_j}\right|^2 = \frac{P_{ij}^2 + Q_{ij}^2}{9(V^R)^2}$$

By calculating $|I|^2R$ in this way, the variables P and Q become the only two results needed from the power flow. Summing this formula up for each phase, each edge, and averaging over all the unique loading conditions m, the objective statement becomes the following:

$$\min \sum_{m \in M} \sum_{(i,j) \in E} w_m \frac{\left(P_{ij}^m\right)^2 + \left(Q_{ij}^m\right)^2}{3(V^R)^2} r_{ij} \qquad (4.1)$$

This objective statement is quadratic over P and Q making the formulation a Mixed Integer Quadratic Program (MIQP).

Constraints

The first constraint to consider is that only one capacitor should be placed at a time. Equation (4.2) ensures that this condition will be met using the variable C.

$$\sum_{i \in V} C_i = 1 \qquad (4.2)$$

Secondly, the power flowing in each section will be constrained similarly to the way it was in the linearized power flow constraints in Chapter Three. Power flowing in each node is constrained to equal to the power flowing out except for the substation bus.

This allows for the circuit to draw as much power as it needs from the bulk electric grid without adding a separate variable to signify power drawn from the substation bus.

$$\sum_{(i,j)\in E} P_{ij}^m = \sum_{(j,k)\in E} P_{jk}^m + \beta_p^m p_j, \forall j \in V, m \in M \tag{4.3}$$

$$\sum_{(i,j)\in E} Q_{ij}^m = \sum_{(j,k)\in E} Q_{jk}^m + \beta_q^m q_j - \sum_{j\in C} Q_j^R - C_j Q_{new}^R, \forall j \in V, m \in M \tag{4.4}$$

Here, a positive value for P_{ij} represents power flowing from vertex i to vertex j and a negative value indicates the opposite. Similarly, a positive value for Q_{ij} indicates a lagging power factor in edge (i,j) and a negative value indicates a leading power factor. Notice that the reactive power flow equation has two additional terms related to capacitors. The first adjusts the reactive power flow for existing capacitors and the second uses the binary variable C_j to allow for the possibility that the new capacitor is located at the vertex j.

Optimal Capacitor Placement Example

Test System 4, pictured in Figure 4.4 (a) on the following page, is the same feeder from which the data set discussed in Figure 4.2 and Figure 4.3 was obtained. This system is the one selected to test the OCP formulation and the BESS location formulation later in this chapter. The feeder, located in a rural area is lengthy with a low concentration of load and, like Test Systems 2 and 3, was received from a local utility. It has (996) nodes, (995) sections, and (592) loads and (2) existing capacitors shown by the green markers in Figure 4.4. The first capacitor is a 600 kVAR fixed capacitor located on the lower branch of the circuit and the second is a 450 kVAR switched capacitor located on the upper branch.

Notice from equation (4.2), only vertices that are potential locations for a capacitor need to be considered in the formulation. Therefore, model reduction can be used to eliminate nodes that are not being considered. Capacitors are typically only located on the

main lines of the feeder, as opposed to laterals, to allow for easy access to the devices and prevent conflicts with protection equipment. Pictured in the bottom-left of Figure 4.4 is the reduced model of Test System 4. For this model reduction, all the laterals have been removed and the combined load associated with each one has been added to the main line vertex that the lateral is connected to. This type of reduction will not affect the power flowing through any of the main line sections while allowing for the power flow in lateral sections to be ignored. The reduced model has (228) nodes, (227) sections, and (162) loads. Each load marker is adjusted in size relative to the amount of load that is attributed to that bus, illustrating where the load concentrations are in the circuit.
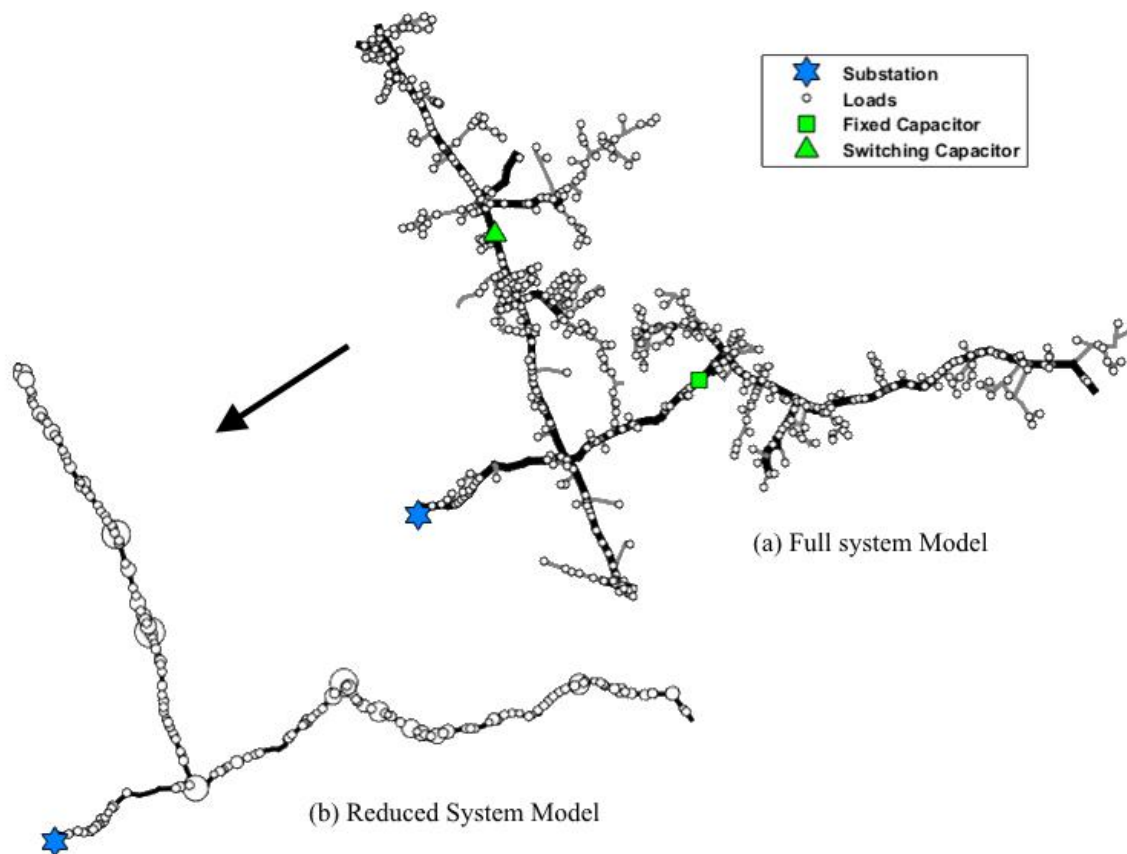
Figure 4.4 – Test System 4 and Model Reduction

73

With both capacitors removed, the problem was formulated first to add a 600 kVAR fixed capacitor and then to add a 450 kVAR switched capacitor. The fixed capacitor location was optimized over (77) unique circuit conditions and the switch capacitor over (33). Using CPLEX through the MATLAB interface on a PC with an Intel Core i5-4590 3.3GHz processor and 8GB of RAM, the solver took 32.2 s and 6.8 s to converge to the optimal solution for the fixed capacitor and switched capacitor respectively. The cyan markers in Figure 4.5 shows the locations that were determined to be optimal.
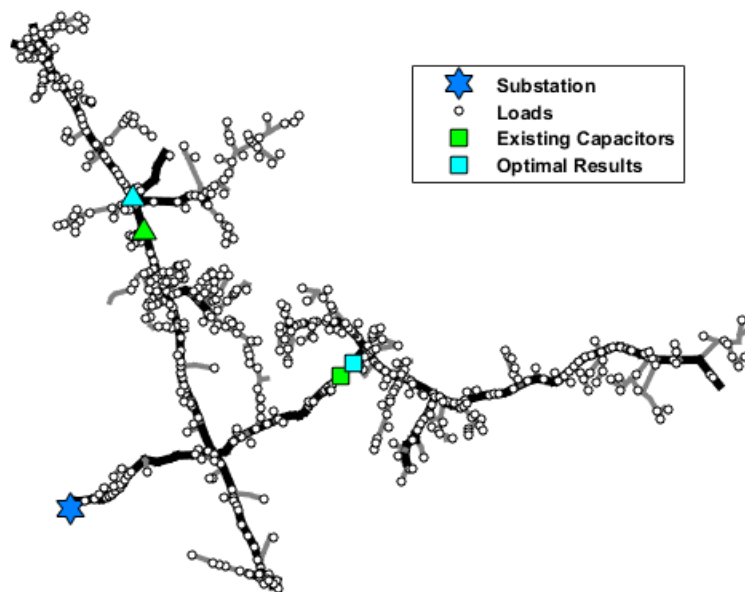
Figure 4.5 – Optimal Capacitor Placement Results

Notice how close the optimal locations are to the existing capacitor locations. These results verify that this OCP method aligns with the method that the local utility used when originally determining the capacitor locations for this circuit. This is an important result because it validates the OCP method by showing the results of the method are reasonable and practical. The next step is to adjust this method so that it can be used to locate a BESS.

74

4.4 - Battery Energy Storage Placement

The biggest difference between a capacitor and a BESS, is that, in addition to providing reactive power, a BESS can consume reactive power, supply real power, and consume real power at any amount up to its rated capacity. This makes the BESS a much more versatile asset than a capacitor which in theory should make it much more capable of reducing circuit losses.

Peak shaving is a simple control algorithm for a BESS that uses energy storage to even out the demand on a circuit over a set time period. This is done by charging the battery during times of lower demand and discharging during peak demand. Since losses are proportional to $|I|^2$, reducing peak current at the expense of raising the minimum current can have a large impact on losses. For this reason, and since it is the purpose of this chapter to determine how the location of a BESS impacts the losses on a circuit, peak shaving will be considered the primary objective for the discussion on sizing and location of the BESS.

BESS Sizing

Like the approach to sizing capacitors, examining the load-duration curves can offer insight on what size BESS is required for a system. For peak shaving, it is important to consider the distance from the minimum and maximum values to the average value of these curves. This value is the power at which the battery will have to charge or discharge to adjust the demand at the head of the feeder. In addition, the area between the average load and the load-duration curve can offer insight as to how much energy storage is required for peak shaving. Note that the total area above the average should equal the area below.

75

Figure 4.6 shows the monthly average load-duration curves for the real power demand on Test System 4 (left) as well as monthly load distribution using box-and-whisker plots for each month (right). From the plots, the largest distance between a minimum or maximum value and the monthly average for any month is around 2 MWs occurring in January, June, July, and August. The maximum area occurs in the months of July and August and is around 4,000 kWh. Thus, for a peak shaving algorithm to be implemented on this circuit, a 2 MW battery with 4,000 kWh of available energy capacity is needed. Note that these size requirements are chosen without considering the effects of PV.
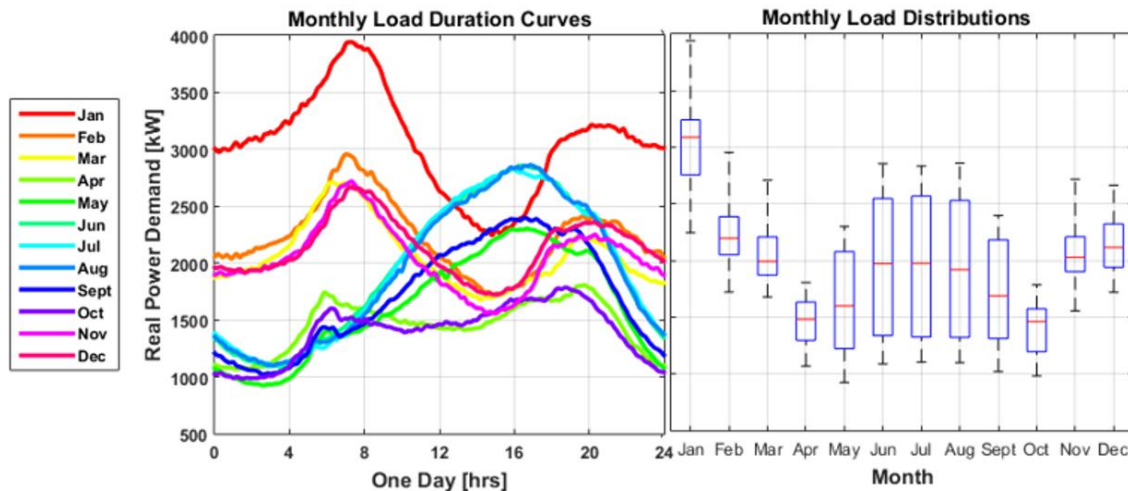
Figure 4.6 – Monthly Average Load-Duration Curves and Distributions

High penetration of PV can have a significant effect on the demand profile of a circuit and consequently, the sizing requirements for a peak shaving BESS. For winter months, load will normally peak around 7:00 or 8:00 AM, trail off in the afternoon, and rise again around 6:00 or 7:00 PM as is the trend during the months December, January, February, and March in Figure 4.6. Since peak generation for PV falls between the hours

of 10:00 AM and 4:00 PM, this afternoon dip is exaggerated forming what is commonly referred to as the "duck-curve." Issues with this are the large ramp-rates required for on-system generation between the hours of 4:00 and 6:00 PM where PV generation is trailing off and load is increasing. Peak shaving with BESS can be an effective way to mitigate this and ease the stress placed on a utilities' generators.
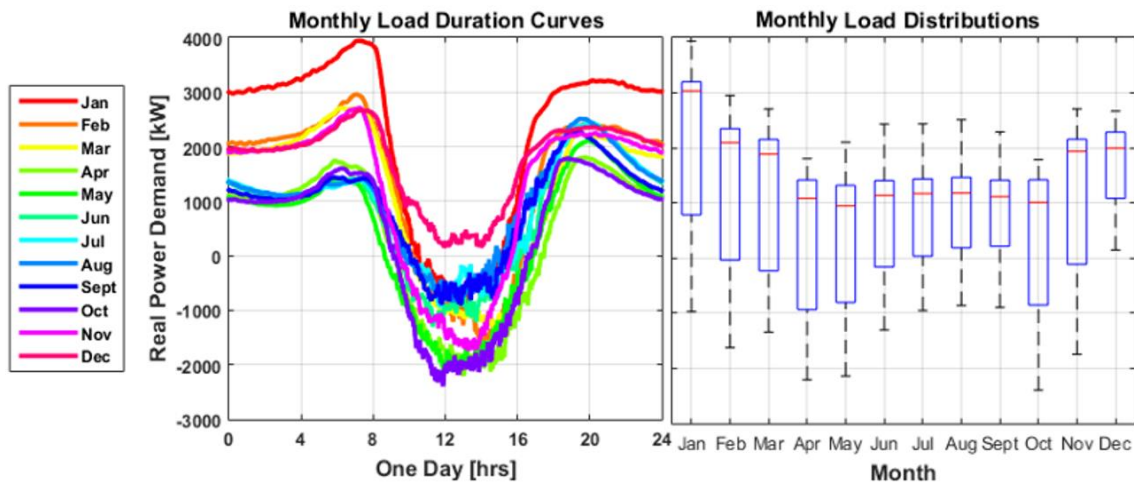
Figure 4.7 – Monthly Average Load-Duration Curves and Distributions with PV

Using another data set containing measured output from a 5 MW PV farm over an entire year, Test System 4's load-duration curves can be adjusted for the addition of a PV farm to the circuit. Figure 4.7 shows the resulting monthly average net demand for the circuit with the PV farm added and provides a good example of the "duck-curve" phenomenon previously discussed. Notice that, due to the relative size of the PV farm and the load, the circuit would regularly experience reverse power flows. Using the same analysis as before, the 5 MW of PV generation roughly doubles the size requirements for

the BESS. As a result, a 4 MW battery with 8 kWh of available energy capacity is chosen for tests with PV present.

Considering the effect that PV generation has on BESS location requires two main additions to the problem. First, a set is required to store all the locations of PV of the circuit.

$$D := \{d \in V : a\ PV\ array\ is\ connected\ at\ vertex\ d\}$$

This will allow for the PV generation to be inserted at that vertex in the power flow equation the same way existing capacitors were accounted for in the OCP formulation. Second, since PV output changes independently from the load, a third dimension is needed in the histogram to find all the unique circuit conditions throughout the year.
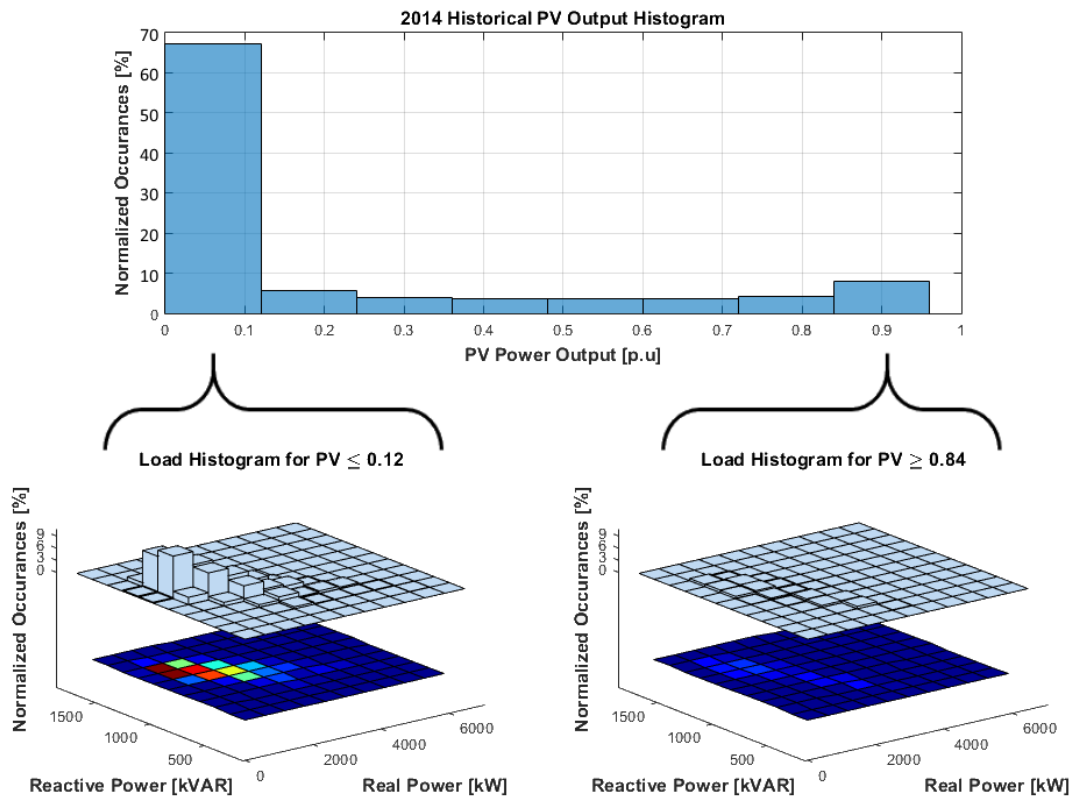
Figure 4.8 – Load Histograms with Added PV Dimension

Figure 4.8 illustrates how the 3-variable histogram works. In the top part of the figure is a histogram of the PV output for the entire year using 8 different bins. The real and reactive power data can be separated out per each PV bin and the 2-varible histogram shown previously can be calculated for the partitioned data. In the figure, the load demand data is divided into 10×10 grids and is shown for the first and last bins corresponding to times when the PV array is either not generating or at full capacitor respectively. Notice that this accounts for over 75% of the year's data. The total number of unique loading conditions that results from this analysis is 800 (10×10×8), however, due to the concentration of the data, this number will be greatly reduced once the empty bins and outliers are removed.

BESS Modeling and Control

The two most important components of the BESS model are the charging/discharging rate (CR/DR) and the state of charge (SOC). The CR/DR describes the amount of power that the BESS is either supplying or receiving from the gird. The values are non-negative and are bounded by the rated power of the BESS (S_B^R).

$$0 \leq CR, DR \leq S_B^R \tag{4.5}$$

Related to the CR/DR are the charging and discharging efficiencies, η_c and η_d. These efficiencies quantify the losses sustained when storing or releasing energy respectively, and include losses from the internal resistance of the battery and the inverter. The round-trip efficiency η for storing and releasing energy is calculated using equation (4.6).

$$\eta = \eta_c \times \eta_d \tag{4.6}$$

The amount of energy stored in a battery is described by the SOC parameter, similar to a fuel gauge in a car. Typically, a battery will have an energy rating C_B in kWh and a maximum depth of discharge (DoD) supplied as a percentage of the energy rating. These provide the upper and lower limits for the SOC given by the following inequality:

$$(1 - DoD)C_B \leq SOC \leq C_B \tag{4.7}$$

The SOC and CR/DR are related by equation (4.8) where SOC_0 is the SOC at time t_0.

$$SOC(t) = SOC_0 + \int_{t_0}^{t} \left(\eta_c CR(t) - \frac{1}{\eta_d} DR(t) \right) dt \tag{4.8}$$

Table 4.1 shows the technical specifications for a 2 MW Utility T&D Advanced Lead Acid Battery Bank. The specifications of this BESS are typical of those for a BESS that would be used by a utility on a distribution system and is provided as an example for the different parameters discussed related to batteries.

Table 4.1 – 1 MW Advanced Lead Acid Battery Specifications

Parameter	Quantity
Output Power Maximum (S_B^R)	2,000 kVA
Total Energy Capacity (C_B)	12,121 kWh
Depth of Discharge (DoD) Maximum	33 %
Available Energy Capacity	4,000 kWh
Discharge Efficiency (η_d)	96.7 %
Charge Efficiency (η_c)	93.0 %
Roundtrip Efficiency (η)	90.0 %

In general, the location of a BESS can be optimized for any control algorithm or combination of algorithms. It is assumed, however, that the control is deterministic based

on the conditions of the circuit and that it is not dependent on the location of the BESS. In most cases, a utility wishing to place a BESS on their system will already have a specific reason for why they are installing the BESS, meaning that the control algorithm they wish to use will most likely already be known. For this thesis, it has been assumed that the primary goal of the BESS is peak shaving, thus, the examples that follows shows how to apply a peak shaving algorithm to the BESS location problem. To apply any other algorithm, the real and reactive power being consumed or supplied should be calculated for each of the loading conditions $m \in M$.

An ideal peak shaving algorithm will flatten out the demand to a constant value equal to the average demand over the period. Equation (4.9) shows the calculation required to determine the battery output as a function of the current load demand $P_L(t)$, the current generation output $P_G(t)$, and the average demand of the circuit P_{avg}. The min and max statements prevent the commanded output from exceeding the rated power S_B^R of the BESS.

$$p_B(t) = DR(t) - CR(t) = \min\left(\max\left(\left(P_L(t) - P_G(t)\right) - P_{avg}, S_B^R\right), S_B^R\right) \quad (4.9)$$

To further reduce losses, the remaining BESS capacity is used to provide VAR support. Equation (4.10) calculates the reactive power required to adjust power factor of the circuit to as close to unity as possible without exceeding the BESS rated power.

$$q_B(t) = \min\left(\max\left(Q_D(t) - Q_C(t), -\sqrt{(S_B^R)^2 - p_B^2(t)}\right), \sqrt{(S_B^R)^2 - p_B^2(t)}\right) \quad (4.10)$$

Note that if $p_B = \pm S_B^R$, then $q_B = 0$. Figure 4.9 shows the results of placing a BESS with the above parameters and control scheme on Test Circuit 4 and simulating a 24-hour period.
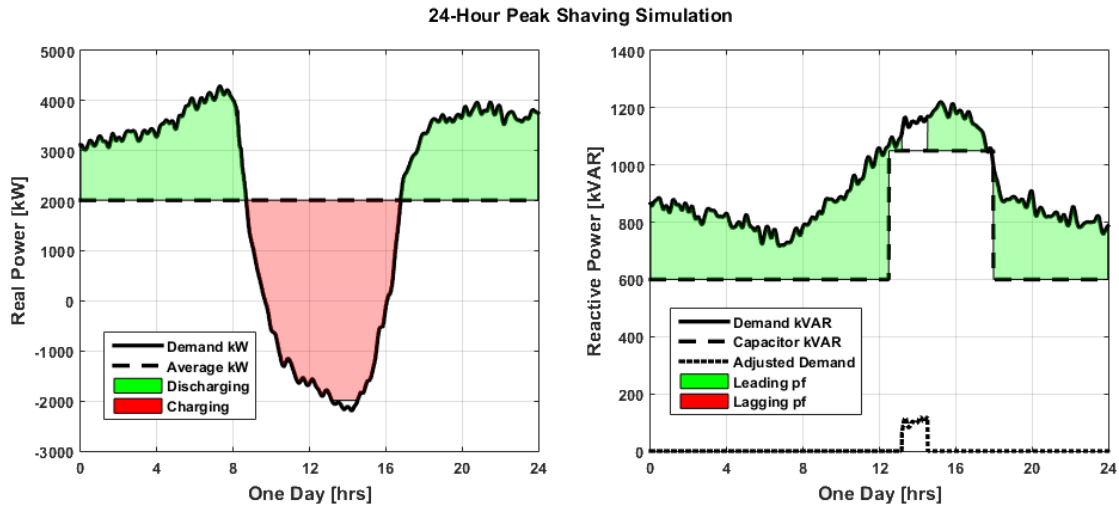
Figure 4.9 – 24-hour Simulation of a Peak Shaving BESS on Test System 4

In the case of peak shaving, it may be true that two equivalent loading conditions result in a different operating point for the battery. This occurs if the average loading is very different over two separate periods, an example of which is shown in Figure 4.10. Here, the circuit demand with PV for Test System 4 is shown for two different days along with the p_B parameter calculated when the circuit's demand reaches 2 MW.
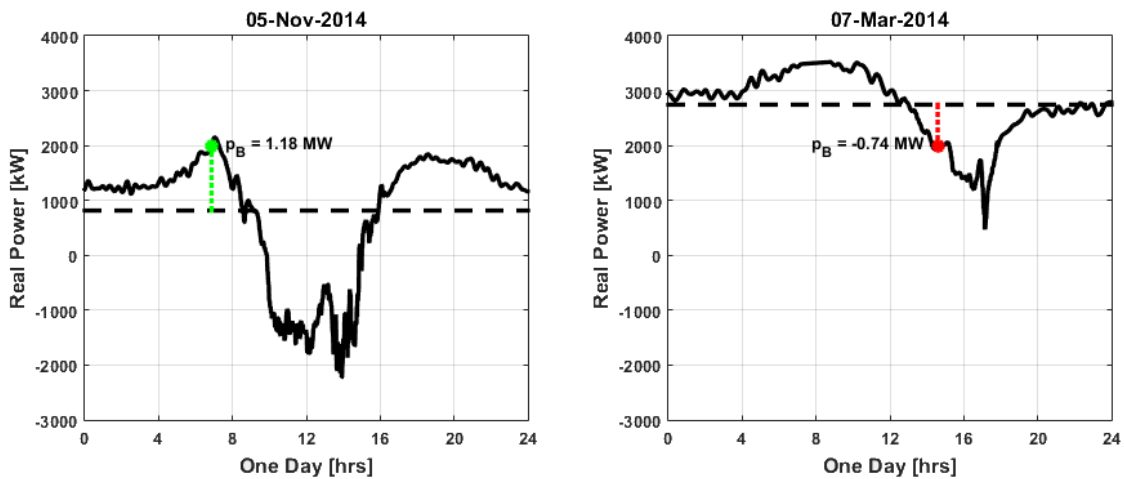
Figure 4.10 – Different Operating Points Resulting from the Same Loading Condition

For November 5th (left), this occurs around 7:00 AM and is during the winter morning peak condition, thus the BESS is supplying power to the circuit. Conversely, on March 7th (right), the circuit is drawing 2 MW around 3:00 PM during the afternoon dip and is charging. For any control where this is the case, the BESS outputs p_B and q_b could be calculated for the entire data set and then added as variables to the load condition histogram in the same way that PV output was added.

Parameters

Since the BESS location problem is comparable the OCP problem, the notation for all the parameters in the previous section is retained for the BESS formulation. In addition to those parameters, the following are also be needed to describe the problem.

p_B^m, q_B^m Real and Reactive charging and discharging rates for BESS at load level m. A positive value for p_B or q_B indicates that the BESS is supplying power to the grid and a negative value indicates it is consuming.

P_d^R Real power rating for the PV array connected at vertex d.

β_d^m Multipliers for the PV array at vertex d where $0 \leq \beta \leq 1$. β represents the per unit real power contributed to the circuit by the PV during load level m.

Variables

The following notation is used to define the variables that are minimized over.

$B_i \in \{0,1\}$ $\forall i \in V$ $= \begin{cases} 1 & Battery\ located\ at\ node\ i \\ 0 & o.w. \end{cases}$

$P_{ij}^m, Q_{ij}^m \in \mathbb{R}$ $\forall(i,j) \in E$ Real and reactive power flowing through edge (i,j) for load level m.

Assumptions

Similarly, the assumptions from the OCP problem should also be made for this problem including the assumptions related to load modeling and power flow. In addition, since power flows are not conducted chronologically, the energy capacity constraints for BESS cannot be enforced in the problem. It is assumed that the battery has enough available storage capacity for the supplied control algorithm to be implemented.

Objective Function

The objective function, shown in statement (4.11), is the same as the OCP. The BESS is being treated as a loss reduction asset, so the goal is to minimize losses.

$$\min \sum_{m \in M} \sum_{(i,j) \in E} w_m \frac{\left(P_{ij}^m\right)^2 + \left(Q_{ij}^m\right)^2}{3(V^R)^2} r_{ij} \tag{4.11}$$

The objective of this chapter is only to apply knowledge from capacitor placement to the BESS problem so only losses are considered. Since there are many other reasons to use a BESS on a distribution grid, it is important for future work on BESS location to develop this objective function to capture all the benefits of storage and not just the reduction of losses. Other benefits may include reduction of voltage flicker, reduction of loading on feeder exit cables or loading on a transformer (preventing the replacement of such items and thus extending their usefulness), reduced ramp-rates required on system generation during evening winter peaks, and increased redundancy for critical loads during outage events. Quantifying these benefits are the key to developing a truly useful method for BESS location.

Constraints

The first constraint is to only place a single BESS on the system constrained using equation (4.12). This is equivalent to equation (4.2) in the OCP problem.

$$\sum_{i \in V} B_i = 1 \qquad (4.12)$$

Likewise, equations (4.13) and (4.14) are the equivalent constraints to (4.3) and (4.4).

$$P_{ij}^m = \sum_{(j,k) \in E} P_{jk}^m + \beta_p^m p_j - \sum_{j \in D} \beta_j^m P_j^R - B_j p_B^m, \forall j \in V, m \in M \qquad (4.13)$$

$$Q_{ij}^m = \sum_{(j,k) \in E} Q_{jk}^m + \beta_q^m q_j - \sum_{j \in C} Q_j^R - B_j q_B^m, \forall j \in V, m \in M \qquad (4.14)$$

These power flow constraint equations vary slightly from the OCP equivalent constraints due to the addition of the new parameters specific to BESS location. For (4.13), a term has also been added to include the power injected by PV generation at each PV bus.

4.5 - Results and Discussion

The reduced model of Test System 4 was again used to test the BESS location problem. All the potential capacitor locations selected in the first section were also considered to be suitable for energy storage, thus the results of the model reduction are the same. Four different test cases were used regarding the level of PV adoption on the circuit: (a) No PV Installed, (b) One 5 MW PV Installed, (c) Three 2 MW PVs Installed, and (d) Distributed 25kW PVs for a total of 5.33 MWs. A 2 MW battery is considered for test case (a) and a 4 MW battery for all other cases.

The cyan markers in Figure 4.11 show the optimal locations that were found for each test case. For test case (a) the results show that the battery is located on the vertical branch of the feeder. This is mostly likely due to the concentration of load in this area of

the circuit. In this case, the battery is active as a buffer between the head of feeder and the load allowing for the battery to reduce the current in the upstream sections.

It is clear from the other three test cases that PV has a great effect on the results. Test case (b) reinforces the idea that for a single utility scale PV farm, it is best to locate the BESS at the PV's point of common coupling (PCC). While not a very interesting result, it confirms that the trivial approach is in fact optimal for this case. Since the PV is the largest single contributor to the power flowing in the circuit, it is reasonable to have the BESS close by to absorb its impact.
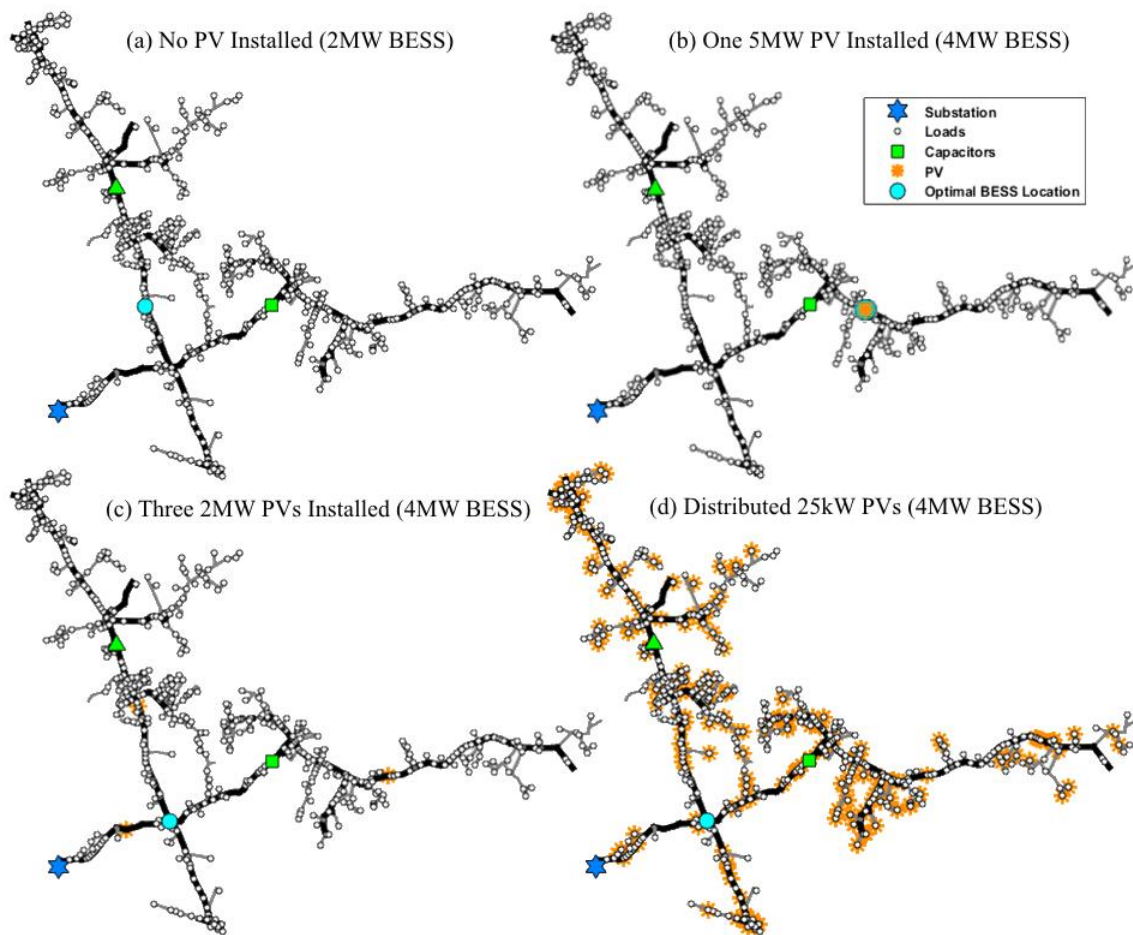
Figure 4.11 – Optimal BESS Locations on Test System 4 with Varying PV Adoption

Test cases (c) and (d) show the result for when the PV generation is not concentrated in a single location. Surprisingly, the optimal location for each is at the same vertex in the circuit. Not surprisingly though, is that this vertex is in a central location relative to the circuits load and the PV. Locating the BESS in this way allows it to have a noticeable effect on the load flowing in more sections of the circuit without having to send power over long distances.

Table 4.2 – Optimal BESS Location Results

Test Case	$|M|$	Solution Time	Daily Energy Savings	Yearly Cost Savings
No PV Installed	139	5.15 min.	7.58 kWh	$332
One 5MW PV Installed	1,033	27.1 min.	103 kWh	$4,510
Three 2MW PVs Installed	1,075	1.31 hr.	45.3 kWh	$1,980
Distributed 25kW PVs	1,040	2.40 hr.	46.4 kWh	$2,030

Table 4.2 shows some more information regarding each test case. Notice the dramatic increase in the number of unique circuit conditions $|M|$ caused by the introduction of PV also resulting in an increase of the time required for CPLEX to converge to a solution. This is a direct result of the added dimension PV gives to the problem. Since a power flow is calculated for each unique condition, this also adds to the computational complexity and thus longer solution times.

Another important result is the energy savings that result from each case. Test case (a) shows little effect in energy savings from the BESS meaning that there is not much value in adding a BESS to the system without PV installed. Since the circuit was designed

to handle the existing load conditions, it is reasonable that there is little benefit to a BESS with the circuit as is. Conversely, the circuit has not been designed for the addition of PV, therefore the energy savings from test cases (b) – (d) show much better results, with the highest savings from test case (b).

4.6 - Conclusion

In conclusion, a BESS location method was developed using ideas established in optimal location of capacitors. While this method does not fully capture the benefits of a BESS, valuable insight was provided by treating the BESS in this way. A BESS was found not to be a good option to consider if the only objective is to decrease losses. There are many other ways to reduce losses on a distribution system which are much more effective and cost much less. Optimal BESS location was found to be sensitive to location of large scale PV on the distribution system. In distributed solar cases, a central location to the circuit's load and PV generation is ideal. It is the author's hope that this work is continued and that many of the other benefits that a BESS can provide are quantified and added to this formulation. This chapter, however, provides a good framework for considerations to be made regarding optimal location of BESS.

CHAPTER FIVE

SUMMARY AND CONCLUSIONS

5.1 - Summary of Work

In this thesis, applications of Operations Research (OR) techniques to distribution

systems were explored. In the second chapter, a Binary Integer Linear Program (BILP) was

formulated to determine the optimal configuration of a distribution system. This BILP was

then tested using several distribution feeder models including an entire substation model.

The partitioning method performed as expected for each test system in a variety of outage

situations and the size of the test system was shown to have a great impact on solution time.

Consequently, system reduction was used for the larger test systems.

In the third chapter, an effort was made to validate the solutions of the partitioning

BILP by checking for overloading of circuit elements and voltage violations. First a

linearized power flow was added to the problem and the voltage and current were

constrained internally to the LP. This magnified the poor performance of the LP for larger

systems and restricted the use of model reduction, however, the linearized constraints were

shown to work desirably for smaller systems. Next, an iterative method was used to solve

the BILP from Chapter Two and then test the voltage and current conditions using efficient

power flow solvers. This method allowed for model reduction and was shown to produce

feasible results for normal operation and faulted scenarios even for larger systems.

Finally, the fourth chapter applied techniques for both sizing and locating

capacitors to finding an optimal Battery Energy Storage System (BESS) design for a peak

shaving implementation. Historical data from the year 2014 was used to optimally place

two capacitors on a test system. The locations were found to be close to the existing capacitor locations on the test system thus validating the capacitor placement method. This method was then developed for the added complexity of a BESS and the locations that minimized power losses on the same test system with varying levels of Photovoltaic (PV) generation added. While this method does not fully capture the benefits of a BESS, valuable insight was provided for optimal location relative to the amount and location of PV on a system. The optimal location was found to be sensitive to large scale PV on the distribution system, whereas in the case of distributed solar, a central location to the circuit's load and PV generation is ideal.

5.2 - Contributions

Partitioning Distribution Systems During Outages

- A BILP was formulated to optimally partition a distribution system containing any number of loops or distributed sources that allows for DG to supply micro-grids islanded from the bulk electric grid, multiple DG to be connected to a single micro-grid, and can enforce that the final solution be radial.

- Topological constraints were developed for the BILP that enforce a graph to be radial by counting the number of vertices, edges, and connected components. These constraints can be used in general in any LP approach to find an optimal radial subgraph of some larger graph.

- A linearized power flow model was applied to a non-directed graph, allowing for reverse power-flow conditions on a circuit, so that constraints on overloading and voltage variation conditions could be added to the BILP partitioning method.

- An iterative, two-step method was developed to enforce overloading and voltage variation constraints externally from the BILP partitioning method that included the development of a constraint that would force the BILP to find a unique solution, used as a feedback loop in the method.

- The importance of model reduction in partitioning a graph was discovered and a simple model reduction technique was developed to group adjacent sections of a distribution circuit that cannot be switched independently from one another.

Optimal Location of Battery Storage

- An Optimal Capacitor Placement (OCP) method was formulated using a MIQP that was shown to produce similar results to the capacitor location approaches used by a local utility.

- A method for using multi-variable histograms to optimize over a large set of data was developed. This was applied to the capacitor location problem to minimize losses over a data set containing a year of data points at 1 minute resolution.

- An optimal BESS location method was adapted from the OCP MIQP that locates a BESS with a pre-defined control scheme on a distribution system such that losses are minimized. This method provides a framework for future study into the optimal location of BESS

- Insight was provided regarding the optimal location of a BESS relative to the amount and location of PV on a system. The optimal location was found to be sensitive to large scale PV on the distribution system, whereas in the case of distributed solar, a central location to the circuit's load and PV generation is ideal.

5.3 - Conclusions

Applying optimization to the design and operation of power systems can provide many benefits to utilities. Ensuring that the electric distribution grid is operating optimally maximizes the return on investments made in the grid by decreasing costs and increasing the usefulness and lifespan of assets. This thesis has used optimization to design solutions to two different problems related to distribution systems that can be applied to any circuit or group of circuits. The optimal reconfiguration method and optimal BESS location method are both great examples of the potential benefits that optimization can provide to utilities. For a power industry with a renewed focus on reliability and efficiency, utilities that understand and use optimization techniques such as the ones discussed in this thesis have a distinct edge over the competition.

REFERENCES

[1]   N. S. Rau, *Optimization principles : practical applications to the operation and markets of the electric power industry*. Piscataway, N.J.: IEEE Press : Wiley-Interscience, 2003.

[2]   M. S. Thomas and J. D. McDonald, *Power system SCADA and smart grids*. Boca Raton, Florida: CRC Press, Taylor & Francis Group, 2015.

[3]   H. L. Willis and W. G. Scott, *Distributed power generation : planning and evaluation*. New York: Marcel Dekker, 2000.

[4]   J. P. Ignizio and T. M. Cavalier, *Linear programming*. Englewood Cliffs, N.J.: Prentice Hall, 1994.

[5]   D. Gomes, R. Colunga, P. Gupta, and A. Balasubramanian, "Distribution automation case study: Rapid fault detection, isolation, and power restoration for a reliable underground distribution system," in *Protective Relay Engineers, 2015 68th Annual Conference for*, 2015, pp. 325-334.

[6]   "Fault Location, Isolation, and Service Restoration Technologies Reduce Outage Impact and Duration," smartgrid.govNovember 2014 2014.

[7]   J. Zhu, "Optimal Reconfiguration of Electrical Distribution Network," in *Optimization of power system operation*, Second edition. ed Hoboken, New Jersey; IEEE Press: Wiley; Piscataway, NJ, 2015, pp. 483-527.

[8]   M. M. Adibi, "Heuristic Search Approach to Distribution System Restoration," in *Power System Restoration:Methodologies & Implementation Strategies*, ed: Wiley-IEEE Press, 2000, pp. 599-605.

[9]   M. Hernandez and G. Ramos, "Meta-heuristic reconfiguration for future distribution networks operation," in *2016 IEEE/PES Transmission and Distribution Conference and Exposition (T&D)*, 2016, pp. 1-5.

[10]   H. T. Yang, J. T. Liao, and X. H. Su, "A fuzzy-rule based power restoration approach for a distribution system with renewable energies," in *Fuzzy Systems (FUZZ), 2011 IEEE International Conference on*, 2011, pp. 2448-2453.

[11]   S. Pal, S. Sen, and S. Sengupta, "Power network reconfiguration for congestion management and loss minimization using Genetic Algorithm," in *Michael Faraday IET International Summit 2015*, 2015, pp. 291-296.

[12]   C. Chen, J. Wang, F. Qiu, and D. Zhao, "Resilient Distribution System by Microgrids Formation After Natural Disasters," *IEEE Transactions on Smart Grid,* vol. 7, pp. 958-966, 2016.

[13]   K. Balasubramaniam, "Optimization Techniques for Modern Power Systems Planning, Operation, and Control," Ph.D., Holcombe Dept. of Electrical Engineering, Clemson University, Clemson, SC, 2016.

[14]   J. Li, X. Y. Ma, C. C. Liu, and K. P. Schneider, "Distribution System Restoration With Microgrids Using Spanning Tree Search," *IEEE Transactions on Power Systems,* vol. 29, pp. 3021-3029, 2014.

[15]   S. Chaitusaney and A. Yokoyama, "Impact of protection coordination on sizes of several distributed generation sources," in *2005 International Power Engineering Conference*, 2005, pp. 669-674 Vol. 2.

[16]   A. C84.1-2011, "American National Standard for Electric Power Systems and
        Equipment—Voltage Ratings (60 Hertz),," ed, 2011.

[17]   S. B. Karanki and D. Xu, "Optimal capacity and placement of battery energy
        storage systems for integrating renewable energy sources in distribution system,"
        in *2016 National Power Systems Conference (NPSC)*, 2016, pp. 1-6.

[18]   B. R. Ke, T. T. Ku, Y. L. Ke, C. Y. Chuang, and H. Z. Chen, "Sizing the Battery
        Energy Storage System on a University Campus With Prediction of Load and
        Photovoltaic Generation," *IEEE Transactions on Industry Applications,* vol. 52,
        pp. 1136-1147, 2016.

[19]   M. J. E. Alam, K. M. Muttaqi, and D. Sutanto, "Mitigation of Rooftop Solar PV
        Impacts and Evening Peak Support by Managing Available Capacity of
        Distributed Energy Storage Systems," *IEEE Transactions on Power Systems,* vol.
        28, pp. 3874-3884, 2013.

[20]   M. Farivar, R. Neal, C. Clarke, and S. Low, "Optimal inverter VAR control in
        distribution systems with high PV penetration," in *2012 IEEE Power and Energy
        Society General Meeting*, 2012, pp. 1-7.

[21]   J. J. Burke, *Power distribution engineering : fundamentals and applications*. New
        York: M. Dekker, 1994.

[22]   S. H. Lee and J. J. Grainger, "Optimum Placement of Fixed and Switched
        Capacitors on Primary Distribution Feeders," *IEEE Transactions on Power
        Apparatus and Systems,* vol. PAS-100, pp. 345-352, 1981.

[23]   P. Kumar, A. K. Singh, and N. Singh, "Sensitivity based capacitor placement: A comparative study," in *2011 6th International Conference on Industrial and Information Systems*, 2011, pp. 381-385.

[24]   P. M. Sonwane and B. E. Kushare, "Optimal capacitor placement and sizing for enhancement of distribution system reliability and power quality using PSO," in *International Conference for Convergence for Technology-2014*, 2014, pp. 1-7.